LAWRENCE
LIVERMORE
NATIONAL
LABORATORY

LLNL-TR-410955

Large Aperture Optics Performance

T.G. Parham, S. Azevedo, J. Chang, A. Conder, G. Heestand, M. Henesian, L. Kegelmeyer, J. Liebman, K. Manes, M. Norton, M. Nostrand, P. Wegner, W. Williams, P.K. Whitman, S. Yang

February 25, 2009

Disclaimer

This document was prepared as an account of work sponsored by an agency of the United States government. Neither the United States government nor Lawrence Livermore National Security, LLC, nor any of their employees makes any warranty, expressed or implied, or assumes any legal liability or responsibility for the accuracy, completeness, or usefulness of any information, apparatus, product, or process disclosed, or represents that its use would not infringe privately owned rights. Reference herein to any specific commercial product, process, or service by trade name, trademark, manufacturer, or otherwise does not necessarily constitute or imply its endorsement, recommendation, or favoring by the United States government or Lawrence Livermore National Security, LLC. The views and opinions of authors expressed herein do not necessarily state or reflect those of the United States government or Lawrence Livermore National Security, LLC, and shall not be used for advertising or product endorsement purposes.

Auspices Statement

This work performed under the auspices of the U.S. Department of Energy by Lawrence Livermore National Laboratory under Contract DE-AC52-07NA27344. This work was funded by the Laboratory Directed Research and Development Program at LLNL under project tracking code 06-ERD-054.

FY08 LDRD Final Report
Large Aperture Optics Performance
LDRD Project Tracking Code: 06-ERD-054
Thomas Parham, Principal Investigator

Abstract

The objective of this work was to improve understanding of the damage performance of large aperture optics under conditions similar to those experienced in large, megajoule-class laser systems. We evaluated large optics at full aperture over a wide range of fluence and intensity, with unconverted light present and with statistical fluctuations typical of large aperture lasers. Specialized optomechanical hardware which edge-illuminated the optics was coupled with a new flaw inspection system and extensive laser diagnostics in an existing large aperture laser system called the Precision Diagnostic System (PDS) to allow *in situ* analysis of damage initiation and growth. Nearby upstream (-z) flaws on neighboring optics was found to be a major contributor to optics damage. Based on results of the initial experiments, improvements were made in the optical configuration and in the optics themselves that significantly reduced their susceptibility to laser-induced damage.

Introduction and Background

Traditionally, the maximum performance of large, fusion-class lasers has been limited by optical damage to their large aperture drive optics. Prior work with large aperture optics under conditions similar to what they will actually experience in regular use unambiguously revealed that significant differences exist between the expected optics lifetime for the large lasers and the projections based on existing damage models.

This work was motivated by the need to understand the primary causal mechanisms that differentiate large-integrated laser damage performance from small-beam damage experiments and, if possible, to develop ways to mitigate them. There are many potential causes for these differences, but we focused on a few that seemed most probable:

- Growth of damage sites is likely a function of both 1ω and 3ω fluence
- Initiation of bulk damage and filamentation is likely controlled by a combination of 1ω and 3ω intensity
- Contrast in the main 1ωlaser beam, both variable and fixed, can result in hot spots in the final optics package
- Near-neighbor flaws just upstream (-z) can cause hot spots due to both linear and non-linear modulation

Because optics are more highly stressed in the 3ω portion of this type of laser, this work focused on 3ω damage, especially as affected by the presence of residual unconverted 1ω and 2ω light. The studies evaluated the performance of newly developed polishing, conditioning and mitigation processes for crystals and silica optics.

Of particular interest was the effect of unconverted 1ω and 2ω light on 3ω damage. Past studies had been largely limited to one wavelength at a time, i.e. 1053nm, 526nm or 351nm light (1ω, 2ω or 3ω). Pump probe measurements have shown that a 4ω (266nm) pump pulse can trigger free-electron absorption of longer wavelength light[1,2], leading to the assumption that unconverted 1ω light on large lasers may play a significant role in 3ω damage. Recent damage testing in a laboratory setting has indeed shown a strong impact of total fluence (1ω + 3ω) on damage.[3,4]

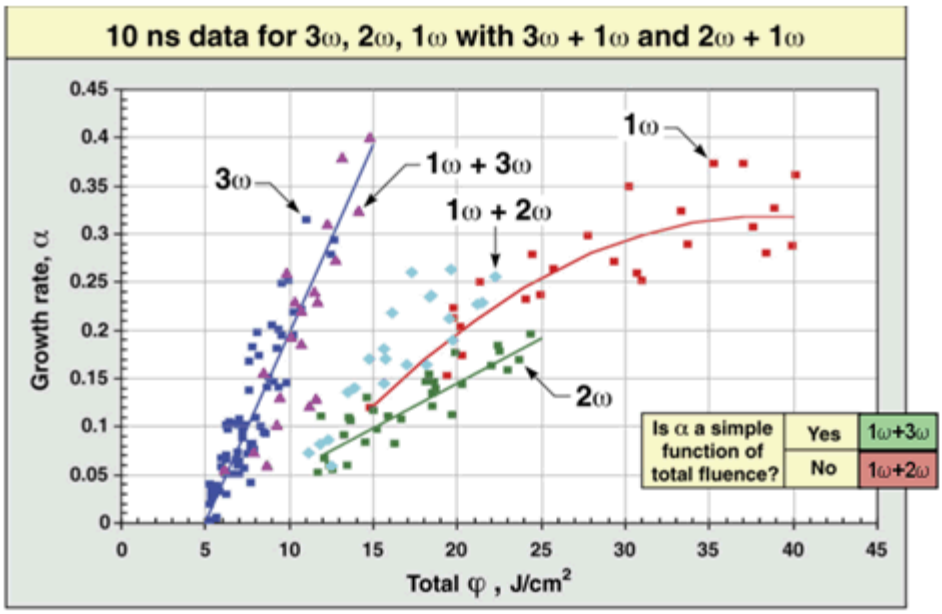

Figure 1: Growth rates of damage on the output surface of silica optics, represented here by exponential growth parameter α as a function of combined 1ω and 3ω fluence. The growth of a damage site is expressed as $D_i / D_o = \beta \exp [\alpha(F)\, i]$ where D_i=diameter of growth site after shot i, D_o= initial diameter, F=fluence in J/cm^2 of 1 ω and 3 ω combined.[4]

In addition, most of the small-aperture experimental data has not taken into account the impact on damage of statistical fluctuations typical of large aperture lasers. Figure 2 is a graphic example of the relationship between the fluence profile details of a large aperture laser beam and the response of the optic under test. Fluctuations in the input beam shown in Figure 2a interacted with the optical surfaces under test as well as with contamination that was present on the surfaces. The convolution of contamination, beam fluctuations and the surface properties of the optic imparted to it by the processes used during surface finishing resulted in the pattern of damage sites shown in Figure 2b.

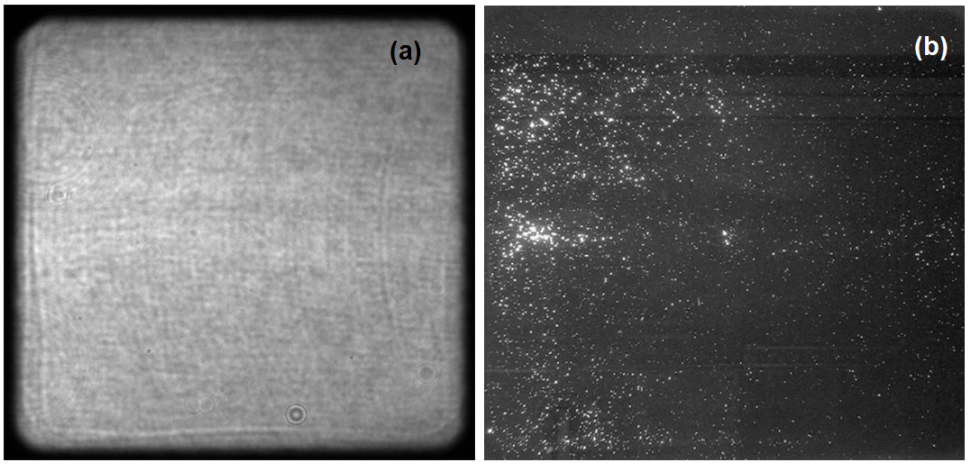

Figure 2: a) Near field image of a large aperture laser beam showing variations in beam intensity (contrast) and b) photograph of an optic showing a pattern of damage sites. There appears to be a statistical correlation of the location of damage sites to the input beam variations.

Comparison of Figures 2a and 2b illustrates the strong dependence of damage on increasing laser fluence in the harsh environment of the target chamber. The fluence differences of the horizontal stripes in the beam profile of Figure 2a represent about 5% of the baseline fluence. This is less than or of the same magnitude as the intensity variations due to contrast that are present in a well-behaved low-contrast 3ω beam. Clearly, small variations in fluence can lead to significant differences in damage.

Although small-beam experiments have yielded much valuable information, it is impossible to quantify damage performance in large laser systems if the effects of unconverted light, beam contrast and shot-to-shot variations are not taken into account.

Experimental Method

For this work we took advantage of a unique test bench called the Precision Diagnostics System (PDS) within the National Ignition Facility to probe optics performance simultaneously at multiple wavelengths, at very large aperture and with beam qualities and optomechanical hardware that are representative of that in a large laser under baseline operational conditions. This system allows one beam from the NIF 1ω (1053nm) main laser to be diverted to a separate location where the 1ω beam may be frequency converted, focused and otherwise conditioned as desired by a set of final optics. PDS provides a wide range of beam diagnostics that are critical for accurately determining the parameters of the input beam (amount of unconverted light, near field image, pulse shape, spectral dispersion, etc.) on a shot-by-shot basis.

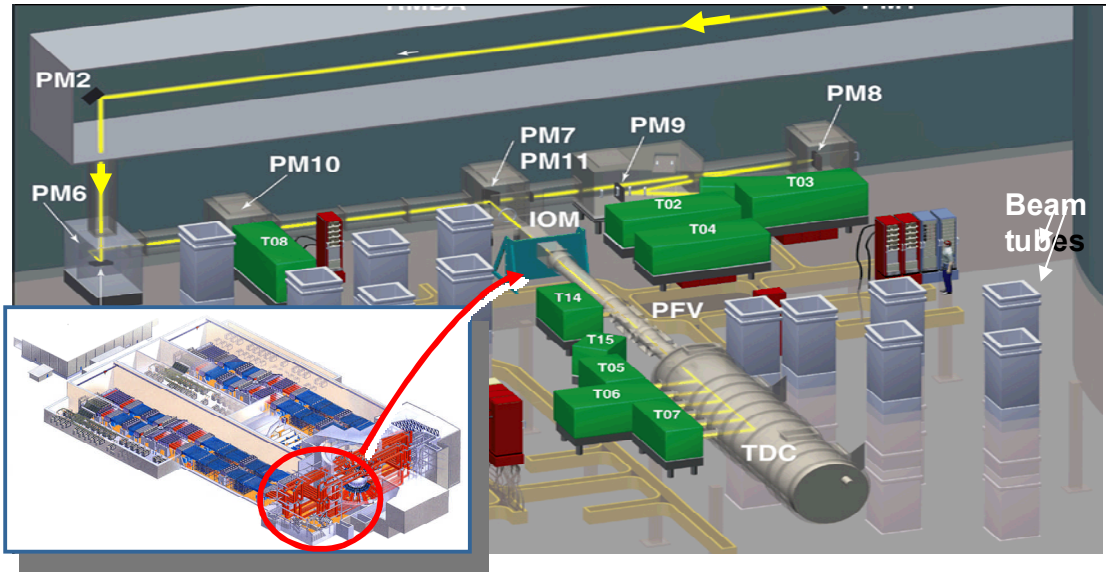

Figure 3. Precision Diagnostic System (PDS) in Switchyard 2 of NIF can re-steer one 1ω main laser beam into a final optics module.

In this work, two generations of hardware and optics were used to evaluate performance of not only the final optics but also the effects of the optomechanical hardware that held them (referred to here as an IOM or integrated optics module)—primarily the spacing of the optics. Lessons learned from the first PDS campaign (PDS 06) resulted in numerous changes in optics and hardware that were validated in a second PDS campaign (PDS 07) and subsequently fielded on NIF (FY08). Most of the shots were conducted for NIF performance verification, with damage analysis "riding along" on the shots.[5,6,7]

A key difference in this work and prior integrated laser tests was the incorporation of extremely high quality *in situ* detection of defects which provided high-confidence detection and tracking of flaws as small as 30μm. This was achieved through a combination of tools:

- A precision telescope and camera (Figure 4) was installed near the focus of the IOM lens to enable accurate *in situ* detection of new and growing damage of sites.
- The IOM provided edge-illumination for the most at-risk optics (SHG, THG, WFL, GDS) to allow individual inspection (Figure 5).
- Optics were laser-inscribed with fiducials around the perimeter (Figure 6) to improve accuracy of flaw location determination both on-line and off-line.
- Flaw tracking software was developed to identify, locate and track flaws shot-by-shot during a campaign and to assist in correlating these flaws to pre- and post-campaign off-line measurements of the optics using a range of imaging tools.

In addition to these four edge-lit optics, backlighting with the NIF alignment beam allowed both bright field and dark field inspection of defects on all of the final optics, though with lower signal-to-noise than that achieved with edge-illumination.[8]

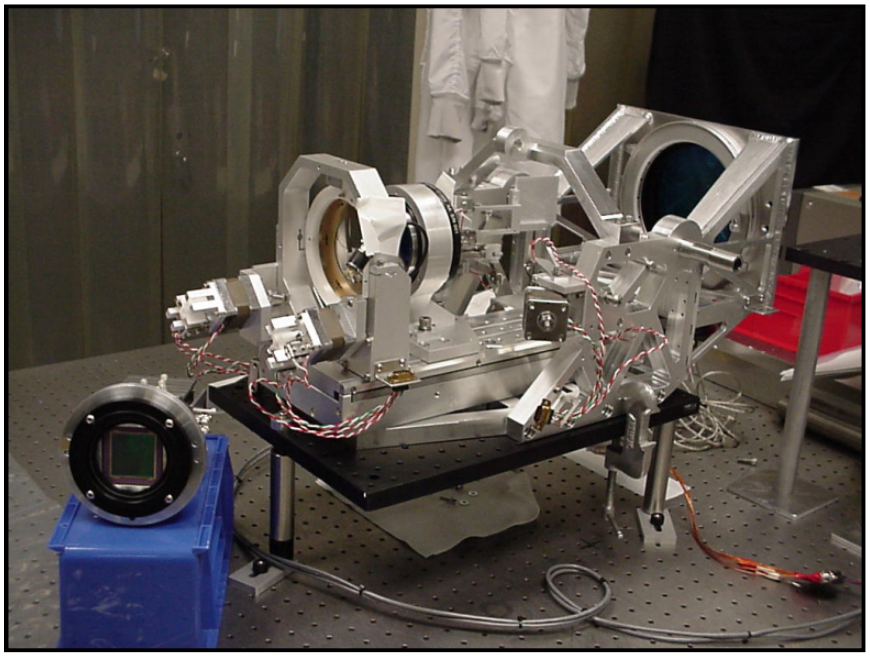

Figure 4: The PDS Final Optics Damage Inspection (PFODI) diagnostic for in situ detection of optical damage sites as small as 30μm in diameter on large aperture (43x43cm) optics.

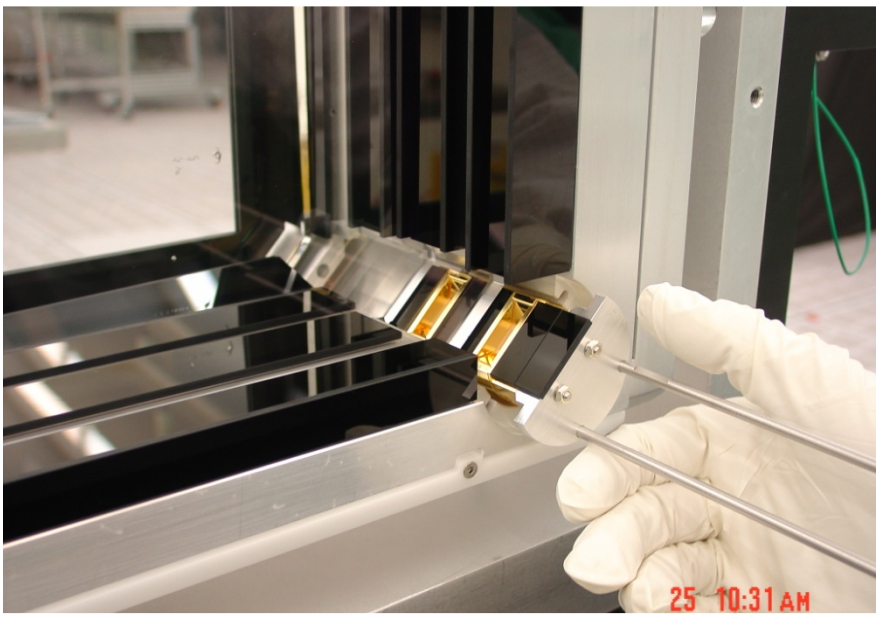

Figure 5: An optical mount for distributing light to the corners and edges of the SHG, THG and WFL optics in the Final Optics Cell (used by the PDS 06 IOM). Light is totally internally reflected, escaping only at sites where damage occurs.

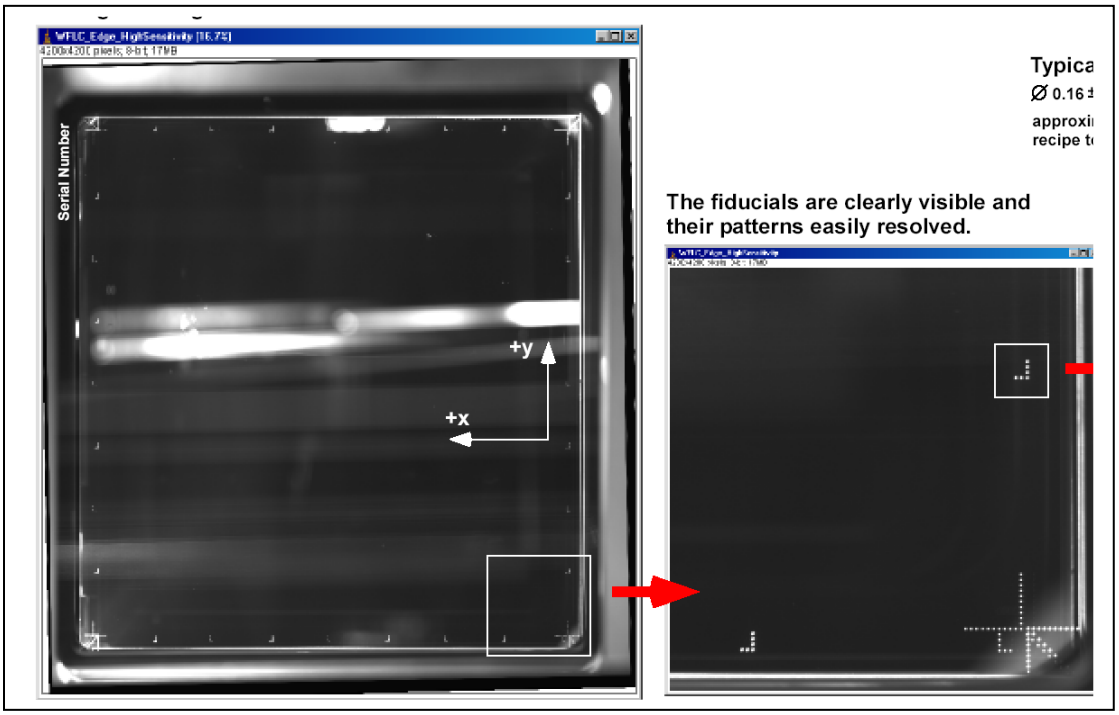

Figure 6: Fiducials added to large optics using multiple pulses of a CO2 laser.

Another key aspect of this study was the matching of local fluence to local damage on a shot-by-shot basis. This was achieved by taking advantage of the extensive suite of laser diagnostics in PDS to characterize the input laser beam for variability over the aperture (contrast), spectral width, pulse length, pulse shape and fluence. The 1ω and 3ω near fields from PDS and the 1ω near field from the NIF Main Laser 1ω Output Sensor Package (OSP) were used to map local fluence to individual damage sites. This shot-by-shot laser exposure data, in combination with the *in situ* measurements of initiation and growth rates was compared to results predicted by existing damage models to provide improved understanding of damage rules, damage morphology and the efficacy of current state-of-the-art optics manufacturing processes.

The optical configuration and the shot data for every shot on PDS, as with all main laser shots on NIF, are permanently archived in databases and file storage systems. This data is most accessible through a web-browser interface to LPOM (Laser Performance Operations Model,[9,10] allowing ready visualization of information such as energies, powers, nearfield and farfield images, etc. for all past shots. A new application, RecycleNow, was developed to register the PFODI observed flaws to the measured near field images in order to track the locations, sizes, and growth histories of damage sites for the edge-lit final optics for each shot. This information is similarly permanently stored, and is also accessible through the LPOM interface. An additional feature of the OI (optics inspection) software and database is a linkage that is established and maintained for every identified site between the site on the optic in question, sites on upstream locations that are spatially correlated, and sites identified using pre-installation metrology that are similarly spatially correlated.

Figure 7 below shows an example of a damage site located, sized and tracked over a series of shots along with the local fluence seen by that damage site during the shot series.

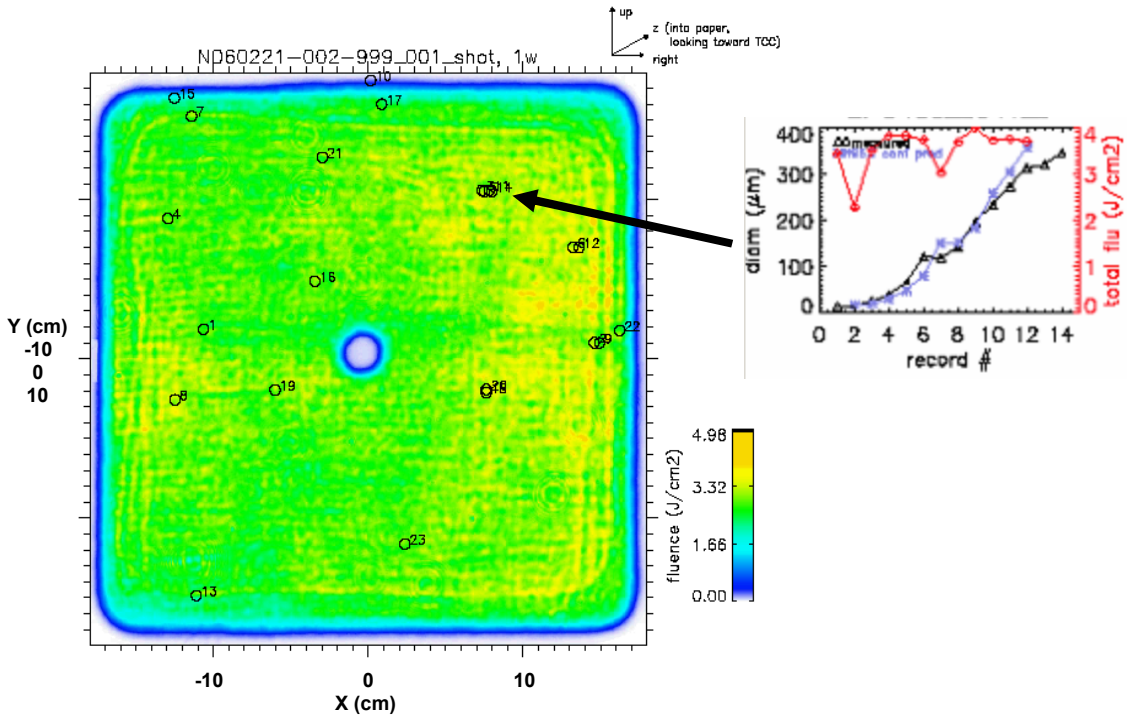

Figure 7: Damage sites on a large-aperture (43x43cm) optic with damage sites mapped to the local fluencies as represented by the 1ω near field. The graph shows the observed vs. projected growth of a damage site vs. 1ω local fluence and shot number.

Configuration for PDS 06 Campaign

The FY06 PDS campaign was based on the optical configuration shown in Fig 8 below which similar to that used in the NIF Early Lights campaigns both on PDS and on the NIF Target Chamber.[11] It included the following optics:

- In the one-atmosphere argon input portion of the IOM:
  - An optional fused silica 1ωCPP (1ω continuous phase plate)
  - An optional KDP (potassium dihydrophosphate) DKDP (deuterated KDP) 1ω PR (polarization rotator) crystal
- A silica target chamber vacuum window (TCVW) separating the argon beampath from an interior volume held at 10 Torr with clean, dry air flowing at one standard liter/minute
- In the 10-Torr interior portion of the IOM:
  - A KDP second harmonic generator (SHG) crystal for frequency doubling
  - A DKDP third harmonic generator (THG) crystal for frequency tripling
  - A silica WFL (wedged focus lens) used to focus 2ω or 3ω light into the target diagnostic chamber (TDC)

- A silica GDS (grating debris shield) which combined a beam sampling grating onto a partial vacuum barrier separated the 10-Torr IOM volume from the high vacuum (10^{-6} Torr) target diagnostic chamber of PDS.
- Not shown in the IOM configuration below, a Disposable Debris Shield optic (DDS) was used in a subset of the shots between the final optics and the Target Diagnostic Chamber.

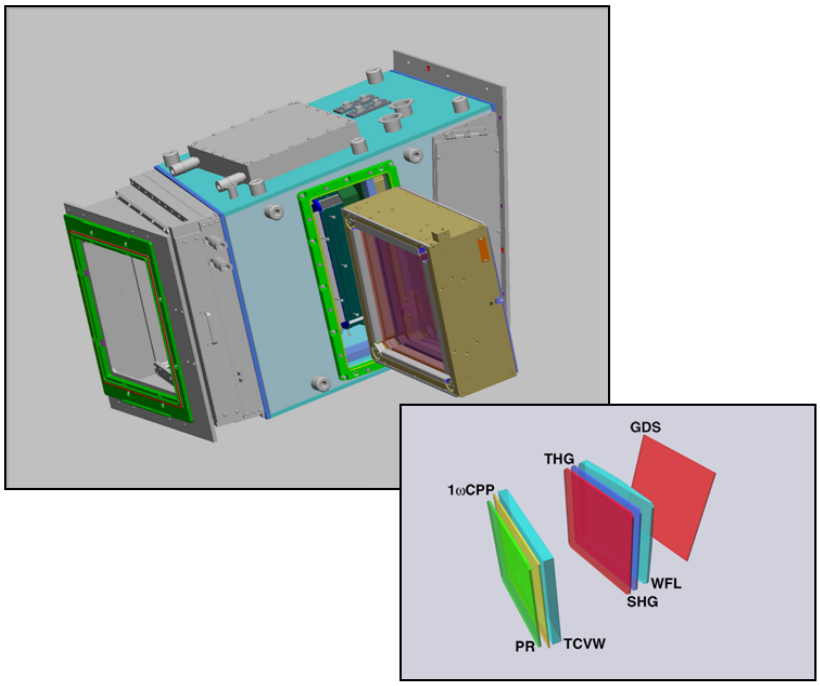

Figure 8. Integrated optics module (IOM) and optical configuration for PDS 06 campaign.

Precision Diagnostic System 2006 (PDS 06) Campaign

Optics for the PDS 06 campaign were selected from NIF production optics that had been polished, conditioned and mitigated with the best known optical fabrication processes and were characterized for defects using a range of techniques. Prior to installation in the laser, the individual optics were analyzed for defects using a commercial optical microscope [ref. summit View] with automated scanning stage capable of providing high resolution (1μm) images as well as the physical location of the imaged defects. This imaging technique was correlated with lower resolution, but more established edge-illumination mapping techniques.[12] For the first time, fiducials were incorporated onto the optics to improve the spatial precision of defect tracking and thus our ability to relate pre-existing flaws to subsequent damage and to track damage growth *in situ* from shot-to-shot. The fiducials were added using laser ablation by a CO_2 laser.

The laser performance during the PDS06 campaign is summarized elsewhere.[5] Over 54 damage-relevant shots spanning the NIF design operating energy and power range were taken on PDS in FY06. Damage was tracked between shots on 14 different large optics:

- Four 1ω Continuous Phase Plates (1ωCPP)
- One Target Chamber Vacuum Window (TCVW)
- One Polarization Rotator (PR)
- One Second Harmonic Generator (SHG)
- One Third Harmonic Generator (THG)
- Three Wedged Focus Lenses (WFL)
- Two Grating Debris Shields (GDS)
- One Disposable Debris Shield (DDS)

After each PDS shot, PFODI images were taken for each of the critical final optics using edge-lighting (THG, WFL, and GDS). Backlit PFODI images were also taken periodically during the campaign on these optics and on the remaining optics (TCVW, SHG, PR and 1ωCPP and DDS when present). Baseline edge-lit and backlit images were obtained whenever new optics were installed and prior to optics removal.

Numerous damage sites were tracked from initiation through multiple shots and subsequently related to shot history, local beam fluences and—very importantly—their spatial relationship to flaws on optics upstream in the beamline.

The ability to track damage initiation in situ and the excellent spatial registration provided by combining PFODI with fiducialized optics allowed traceability between flaws on upstream optics and damage events on downstream optics. Many examples of "fratricide" were observed where damage initiation and growth were driven by hot spots created in the beam by these nearby upstream flaws. A particularly offensive flaw is shown in Figure 9 below. The defect was a particularly large "sleek" created when a particle interacted with the MRF (magnetorheological finishing) tool during final fabrication of the phase plate.[13]

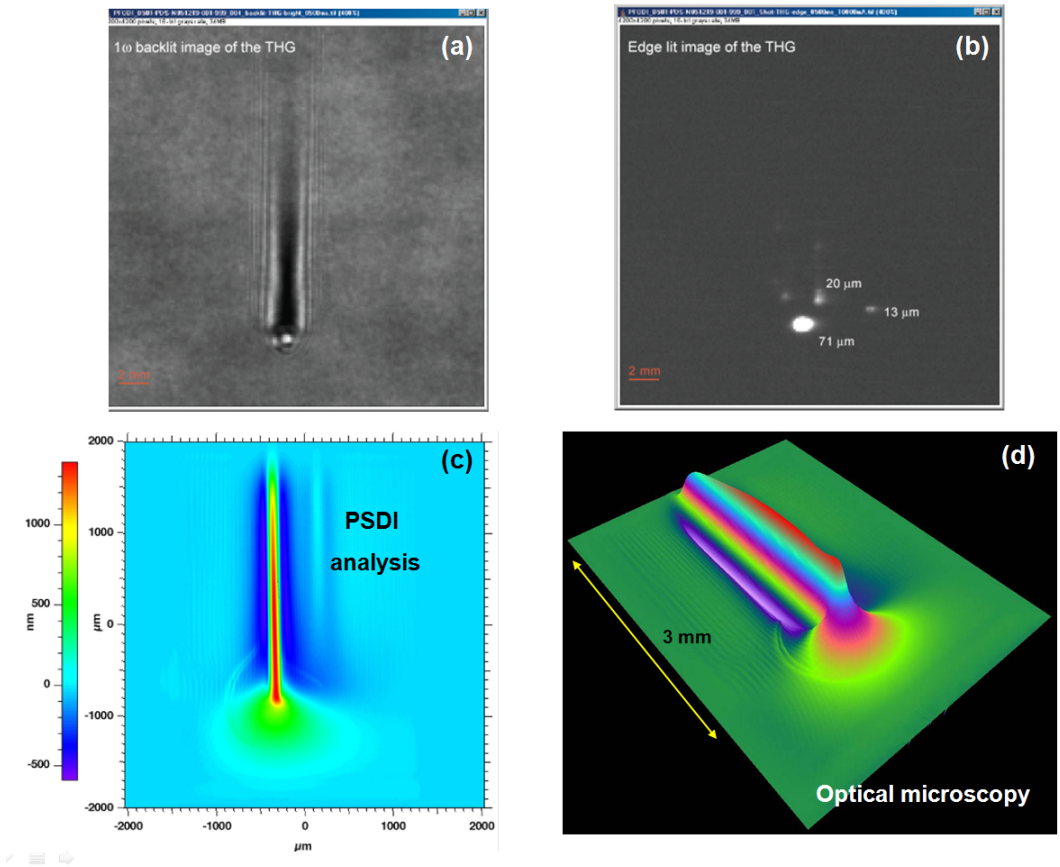

Figure 9: (a) the PFODI bright field view of a manufacturing flaw on a 1ωCPP; (b) damage induced downstream on the third harmonic generator after one relatively low fluence shot due to beam modulation from the flaw. (c) Off-line PSDI phase map and (d) optical microscopy (post-campaign) of the flaw showing that it protruded up from the surface with an OPD of about 500 nm.

This particular flaw was not detected during pre-campaign off-line characterization, but was obvious in PFODI backlight bright field images. The on-line images were used to estimate downstream modulation from the phase defect (Figure 10 below), which varied from 2x to 3x.

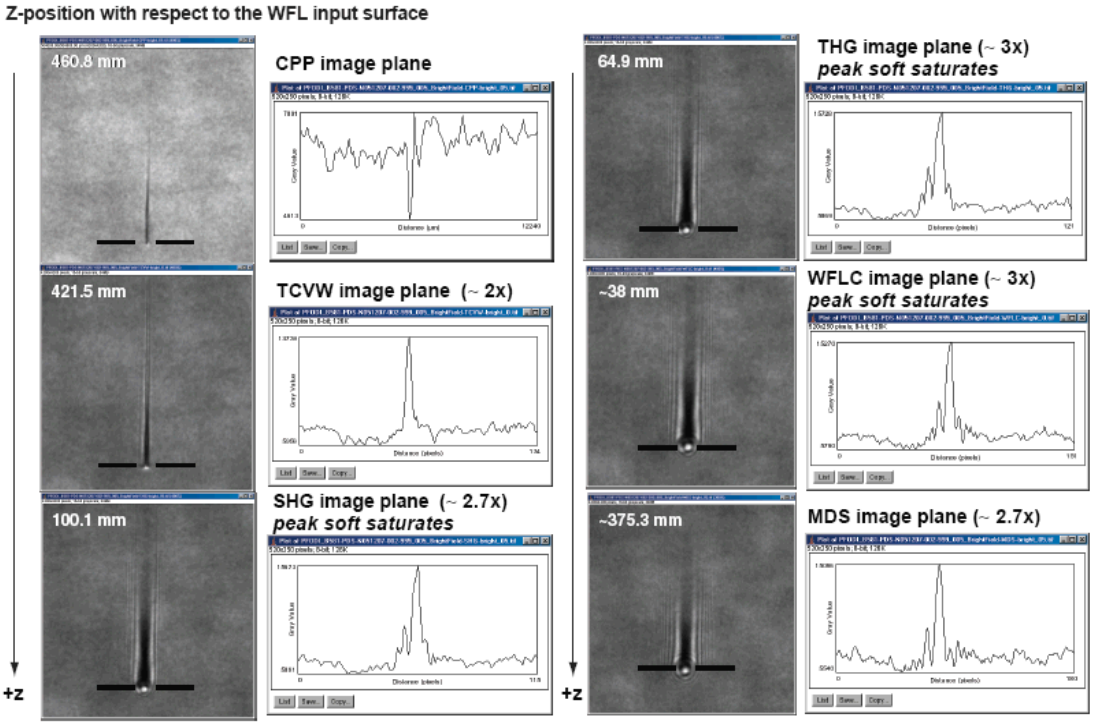

Fig 10 Backlit bright field images of a large phase defect on a 1ωCPP provided modulation estimates for this flaw, but led to an underestimate of the damage that would result from a relatively low fluence shot.

Based on the PFODI measurements, a decision was made to take the next campaign shot (nominally 3 J/cm^2 3ω at the WFL). The SHG, THG and WFL were each damaged in a single shot. Figure 11 below overlays the observed damage site with a post-campaign propagation modeling based on post-campaign PSDI (phase shifting diffractive interferometer)[14,15,16] measurement (Figure 9(c) above). This analysis made clear that simple linear diffraction as estimated from the PFODI bright field was an inadequate metric for the damage impact of upstream phase flaws. It also showed the utility of PSDI measurements coupled to propagation modeling.

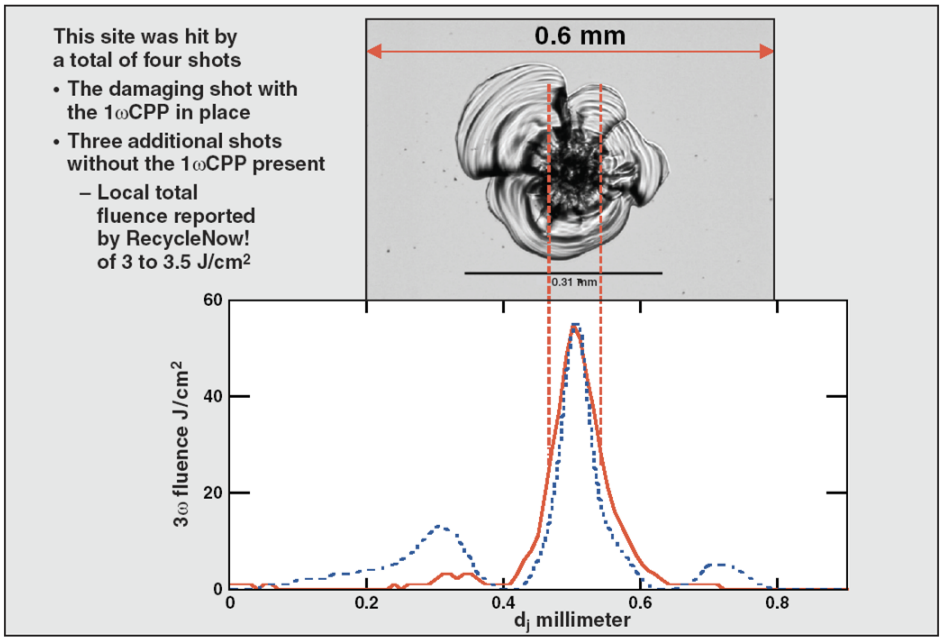

Fig 11. Post-campaign optical microscopy of 1ωCPP phase defect (a) and the local fluence based on post-campaign propagation modeling (b) explained why this particular flaw was so deadly to downstream optics.

After completion of the campaign, all of the optics were removed from PDS and characterized extensively. Observation of damage initiation at the same spatial location (x,y, and z) for sequentially installed wedged focus lenses (WFLs) during the campaign motivated investigation of the spatial correlation of all flaws on upstream (-z) optics to damage on downstream (+z) optics. Flaw correlation used a combination of PFODI images, DMS images, and VIEW optical microscope images and maps. Confirmation of the correlation between flaw and laser damage came through measurement of the phase and intensity of the fratricide 'source' using PSDI. Figure 12 below shows two example phase flaws as mapped. Surprisingly, over half of the large, growing damage sites on the WFLs were associated with flaws on upstream optics—in some cases on the input surface of the lens itself (Figure 13 below). Phase flaws included sol gel antireflection coating defects and laser mitigation sites as well as MRF-induced phase "sleeks" on the 1ωCPP.

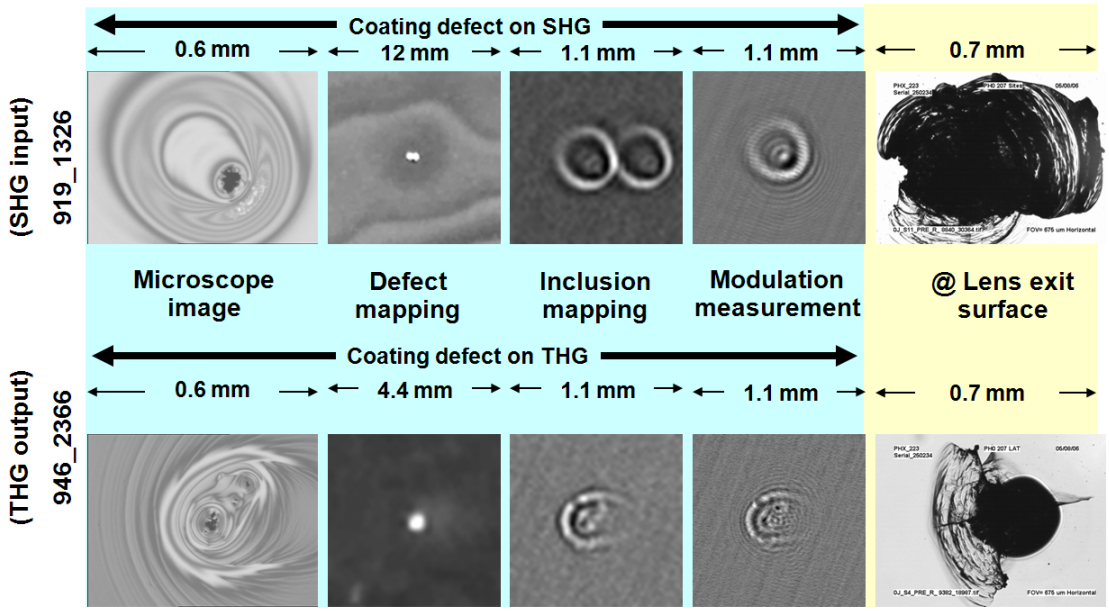

Figure 12. Small defects on nearby optics "upstream" optics (-z) were correlated to damage sites using a combination of fiducials, in situ detection and post-campaign microscopy. Existing models explained lens damage from SHG input coating flaw (defect 919_1326), but failed to explain lens damage associated with THG output coating flaw (defect 946_2366).

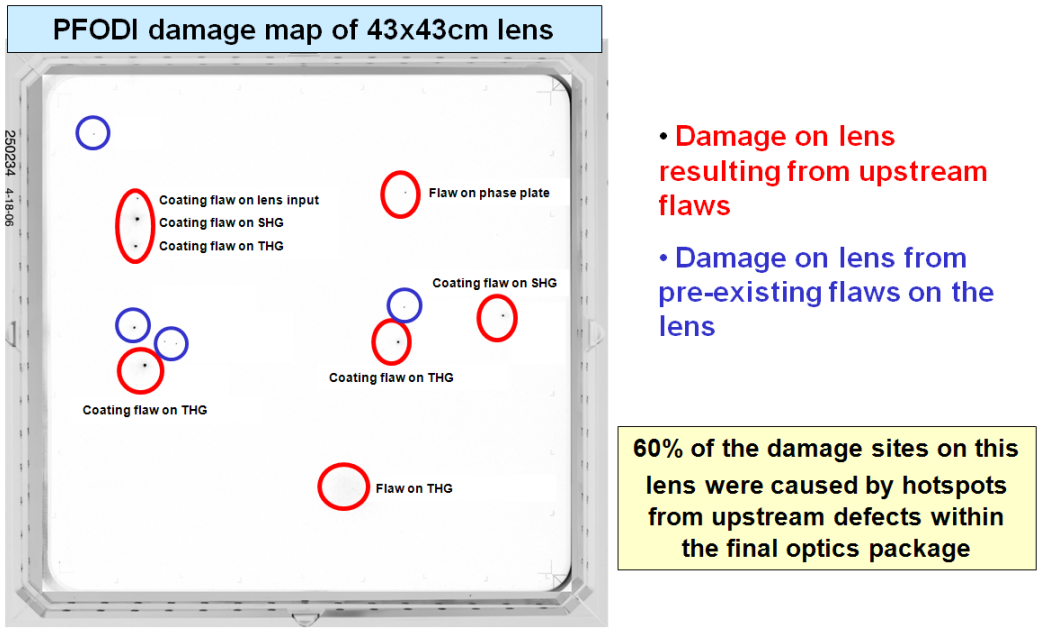

Note: Damage sites shown are the largest, but do not represent all the growing sites

Figure 13. Hot spots due to defects on upstream optics dominated as a source of damage for fused silica optics during the PDS 06 campaign.

In addition to analysis of on-line damage data, post-campaign analysis has posed a challenging question about the physics of filamentation in optical materials. A number of

examples were observed of filamentary collapse at sites on the focus lens where 3ω fluences were not high enough to cause filamentation based on existing propagation models (Figure 14). This may imply 1ω and 2ω fluences are also relevant for filamentation.

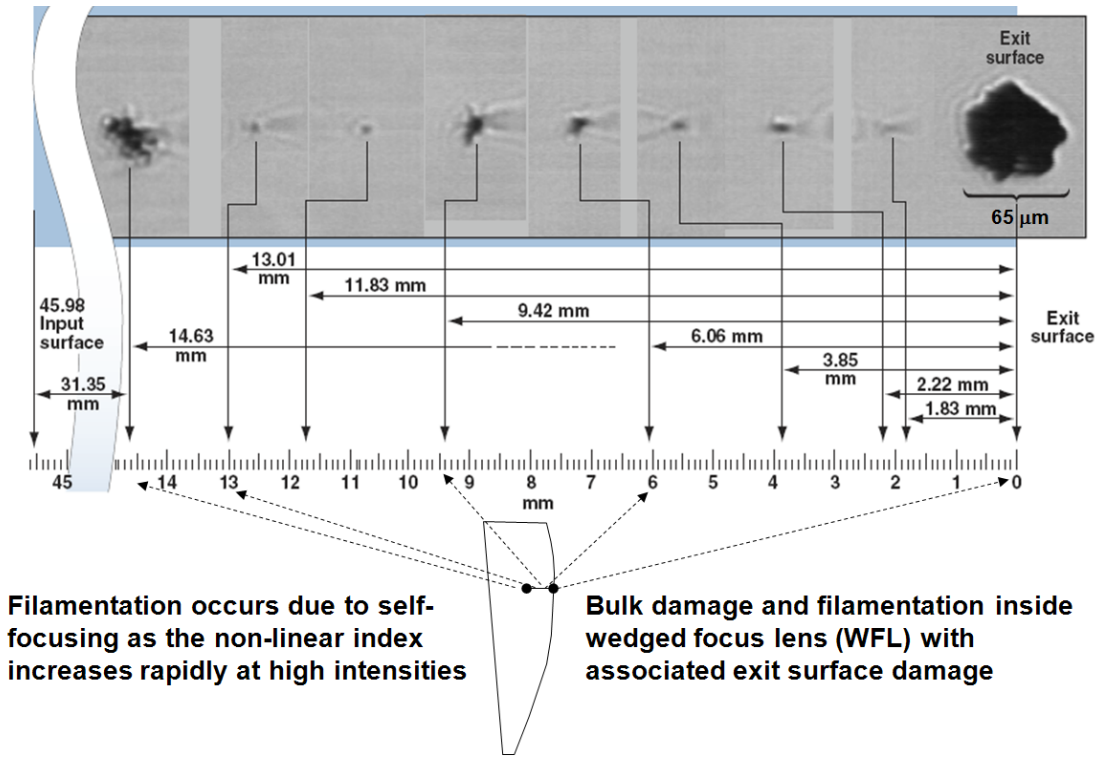

Fig 14. Bulk damage and filamentation were observed at intensities much lower than could be explained with 3ω-only models.

GDS Grating-specific Damage observed in the PDS 06 Campaign

A completely novel type of damage on the GDS (grating debris shield) occurred on the last two shots of the PDS 06 campaign at 1.8 MJ-equivalent (~8 J/cm^2, 3ω). These two shots were taken with the SSD (spectral smoothing by dispersion) bandwidth turned off, suggesting that the damage was caused by SBS (Stimulated Brilloiun Scattering).

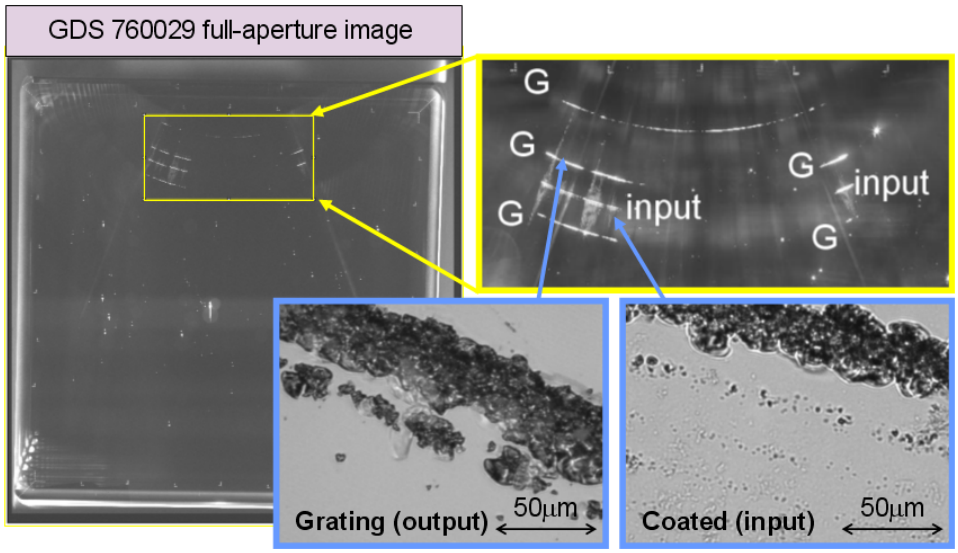

Figure 15: Full aperture PFODI image of the GDS showing damage along the grating lines that appeared on the last two shots of the FY06 PDS campaign. Optical micrographs identify damage lines on the uncoated output surface (containing the beam sampling grating) and the sol gel-coated input surface (no grating).

Figure 15 above shows the damage which was observed growing along the beam sampling grating lines on the output surface and in a correlated fashion on the input surface where there is no grating. The beam sampling grating is a curved grating designed to focus 0.2% of the forward-going 3ω light onto a calorimeter outside the beam aperture. The holographically-imaged, HF-etched grating is ~20nm deep and has variable-width (2-5 μm) spacing following the curve observed in the damage map.

Key conclusions from the PDS 06 Campaign

1) Most of the damage on fused silica optics in the 3ω section of the laser was driven by modulation from flaws on upstream optics—referred to subsequently as fratricide.
2) Filamentation was observed in fused silica optics at main laser intensities much lower than expected based on modeling and prior work on Beamlet.[4]
3) 1ω+3ω growth rules, on average, are consistent with online observations.
4) A novel type of grating-related damage was observed on the GDS during the last two shots of the campaign which were presumed to be SBS-related.

Response to the lessons learned in the PDS 06

In response to the results of the PDS 06 campaign, three efforts were spawned:

1) the final optics package was re-designed with the goal of minimizing key optics susceptibility to non-linear effects,

2) the propagation codes which were used for modeling non-linear effects were upgraded to account for multiple wavelength cross-phase modulation,

3) a suite of enhanced optics production metrology and analysis tools was developed and implemented to enable identifying (and eliminating) all potential fratricide-inducing flaws.

1) Modify the PDS optical configuration

In preparation for a second campaign in FY07, we outfitted PDS with new optomechanical hardware IOM (Integrated Optics Module) that incorporates optics spacings selected specifically to minimize vulnerability to fratricide from upstream flaws. The configuration was selected in late FY06 based on a preliminary library of defects likely to be present in a large laser system. These included digs and coating defects, fused silica bulk inclusions, mitigation sites and the large flaw created on a 1ω continuous phase plate (1ωCPP) by the magnetorheological finishing (MRF) process (Figure 9 above)

Three types of modulation were considered:

- Linear diffraction
- Sum Frequency Generation ($\chi^{(2)}$)
- Optical Kerr Effect ($\chi^{(3)}$)

A wave-vector point model was first used to determine locations within the final optics package where non-linear image formation would occur based on presumed defects on each of the optics in the configuration. The optics were moved to minimize vulnerability to the non-linear images (Figure 16).

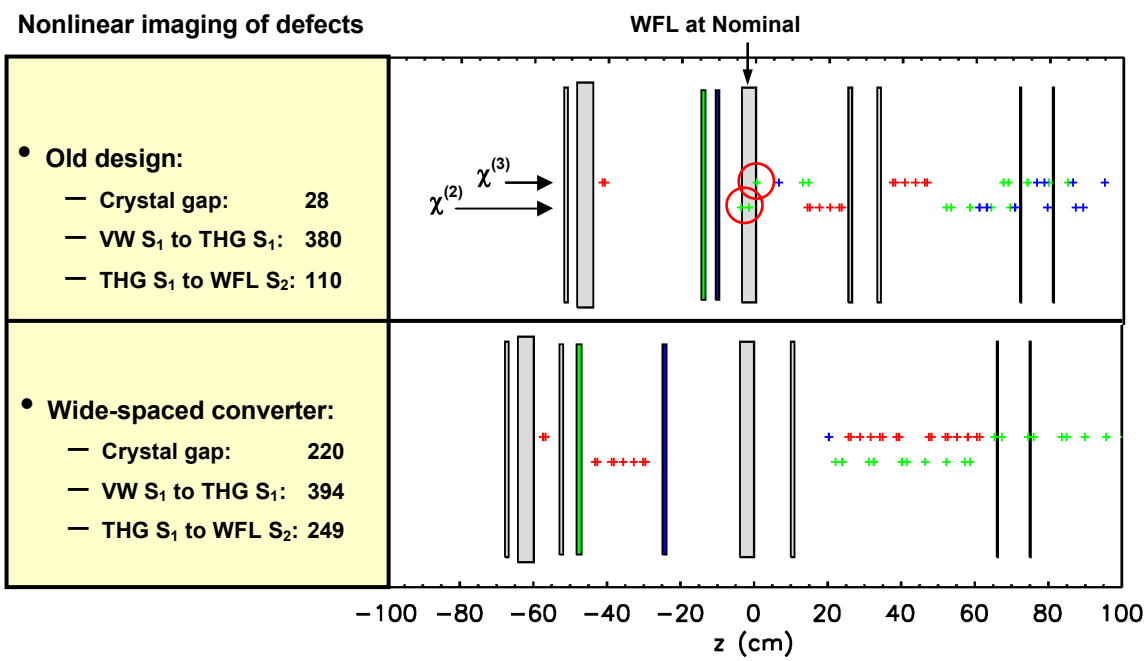

Figure 16: Locations of non-linear images downstream of canonical flaws based on a point model. Colors of the diamonds represent the wavelength of the image.

The point model was validated through PROP modeling (LLNL's primary laser propagation code). An example of the impact of coating defects on the THG on intensification inside the WFL is shown below in Figure 17.

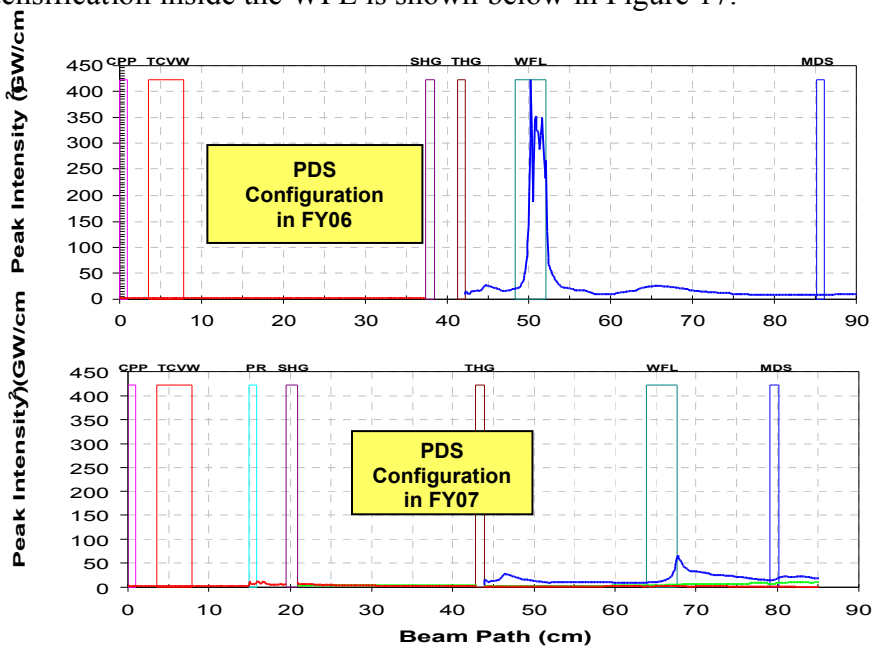

Figure 17: Optical configuration used in the FY06 PDS work compared to the new configuration selected for FY07. This PROP calculation shows the intensity inside the wedged focus lens (WFL) caused by a coating defect on the third harmonic generator crystal (THG) when exposed to a 3.5 GW/cm^2, 1 ns, 1ω input drive.

It is important to note that the new optical configuration balances the threats from types of defects thought most likely for future optics as well as the range of missions expected for large laser systems such as NIF. The configuration is required to be robust against likely defects for high power (represented by a 3.5 GW/cm^2, 1 ns 1ω drive) as well as high energy (represented by a 21 ns shaped Haan pulse, 8 J/cm^2 at 3ω)

As an example of the balance required, the design chosen decreases the vulnerability of the wedged focus lens (WFL) to coating defects and digs on the frequency conversion crystals by separating the second and third harmonic generator crystals (SHG, THG) and by increasing their distance from the WFL. This actually increases the vulnerability of the WFL to phase defects on the vacuum window (TCVW, or Target Chamber Vacuum Window for PDS) and the 1ωCPP. Consequences of this design tradeoff became important later in this work and are discussed below.

Figures 18, 19 and 20 show the new optical configuration and acronyms, a photo of the IOM installed in PDS and a view of the lightweight alumina mounts required to maintain tolerances on the frequency conversion crystals in the wide-spaced frequency converter configuration.

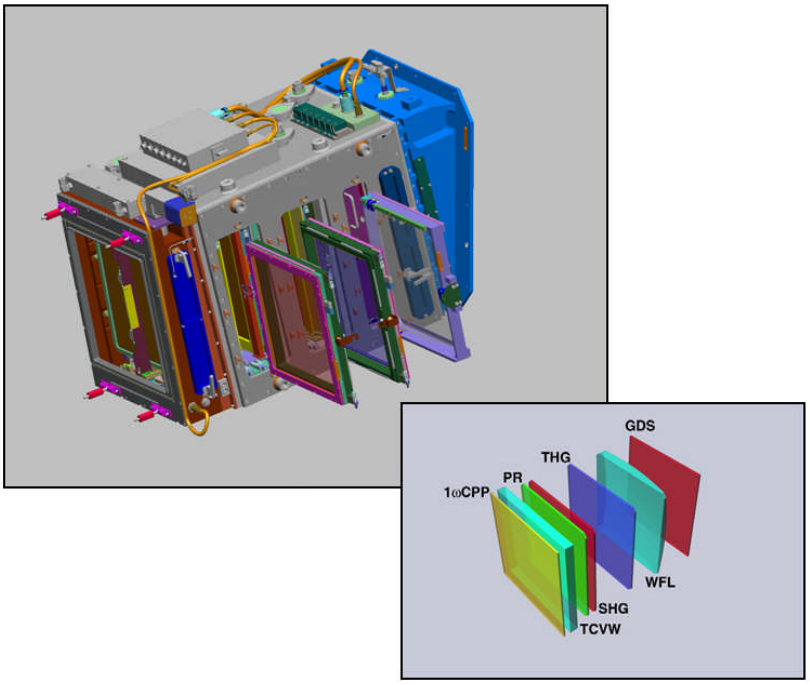

Figure 18: Integrated optics module and optical configuration used for PDS 07 campaign.

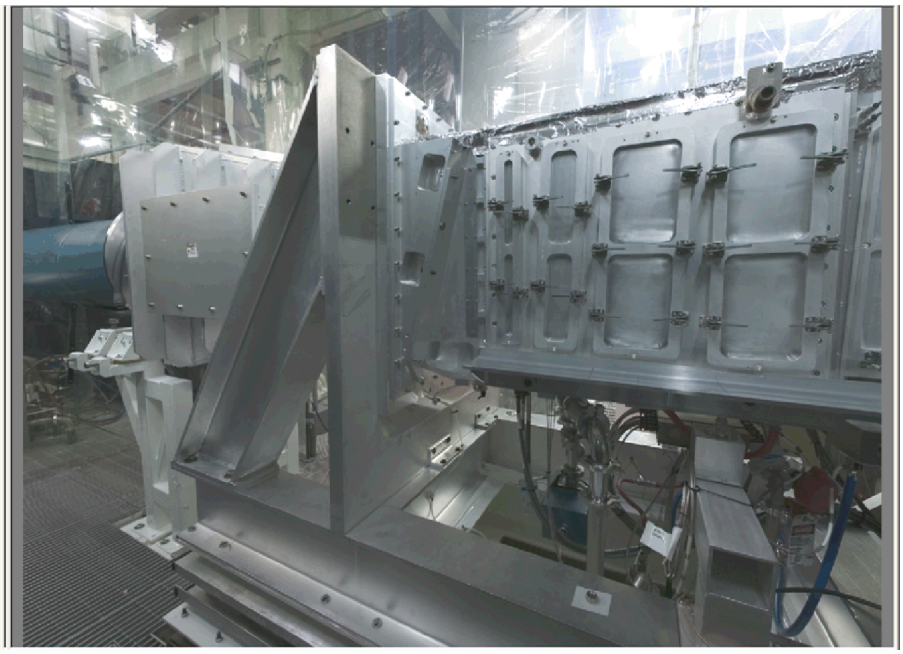

Figure 19: New IOM installed in PDS (Precision Diagnostic System)

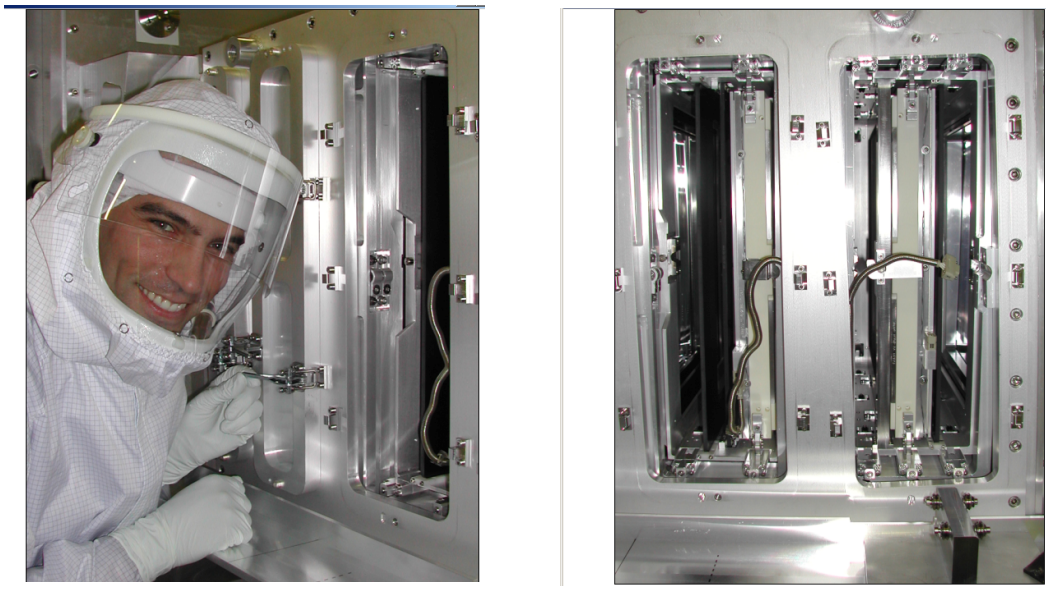

Figure 20: The wide-spaced frequency converter required a new approach for holding the frequency conversion crystals. Lightweight ceramic (alumina) mounts were used to meet the exacting flatness and alignment accuracy requirements.

An additional advantage of the new wide-spaced frequency converter is that it allowed room to include a new edge-illuminated slot between the second and third harmonic generator crystals (not shown in Figure 17). In subsequent work, this will provide insight into performance of fused silica optics when exposed to combined 1ω and 2ω fluences.

2) Upgrade propagation codes

In general, the index of refraction of all optical materials is dependent on the intensity of the light propagating through them. That is, a material whose refractive index is approximately given by a constant, n, at low intensity will often have a larger effective index of n + (gamma)*I at high intensity. The constant gamma is a property of the material. The effect of the nonlinear term gamma*I is usually to increase the index in regions of the beam where the intensity is already high, thus refracting additional light into that region like a small lens. Because this nonlinear refraction is caused by the beam's own intensity, it is called self-focusing, and, if not controlled, can have destructive consequences for optics exposed to high intensity in laser systems.

In the past, our propagation models could only simulate a single wavelength of light, typically 3ω, in the portion of final optics downstream of the frequency converter crystals. This is an approximation, because there is always residual 1ω and 2ω light present, and the intensities in these other two fields can also increase the refractive index experienced by the 3ω field through the process described above. Generally, the optical material responds differently to each wavelength, so the nonlinear coefficient, gamma, will be different for each of the three colors of light. A cross-phase modulation matrix supplies the needed coupling between the three fields present; however, several matrix elements are uncertain and prior work on Beamlet suggested that this coupling is often unimportant.[17] When filamentary bulk damage was confirmed where none was thought

to be possible in the course of this project, we were alerted that LLNL's propagation codes needed attention.

The approximation of simulating only the 3ω beam in the final optics will be accurate if either the intensity or the nonlinear coefficient, gamma, for the 3ω beam is much, much larger than for the other two wavelength beams. To check this assumption, the LLNL propagation codes, PROP and VBL, were modified so that the codes could simultaneously calculate the values of three electric fields, 1ω, 2ω and 3ω, within an optical material. Furthermore, the three fields are not calculated independently, but instead are coupled together through a matrix of nonlinear indices, Γ. That is, the refractive index experienced by each field is calculated as the sum of the conventional linear index of the material, plus the nonlinear contributions produced by its own intensity coupled to those of the other two fields. Coefficients for the matrix of nonlinear indices were based on information found in the available literature.

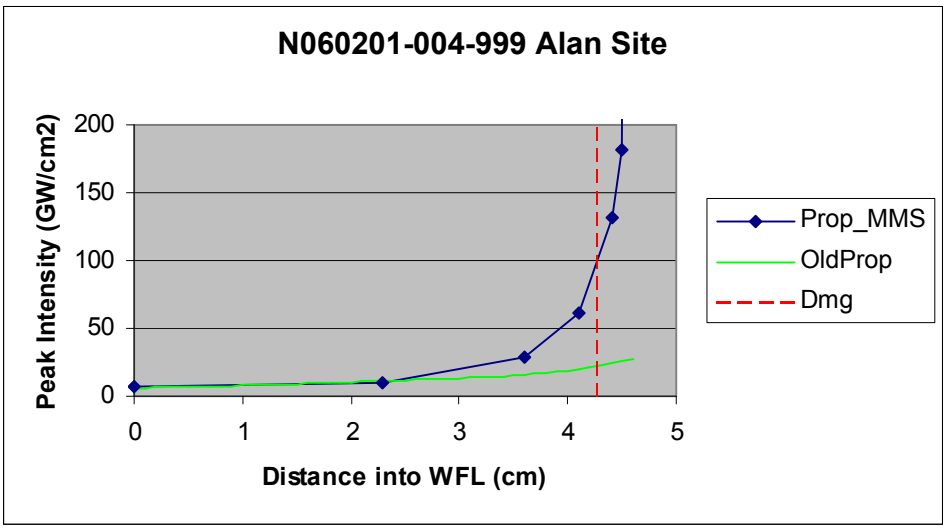

Figure 21: Peak intensity vs. propagation distance into the lens (WFL) for PROP with and without addition of cross phase modulation. Red dashed line shows position where damage was observed.

The results of this code enhancement are shown in Figure 21. The plot shows a calculation of the peak intensity as a function of propagation distance into the Wedged Focus Lens (WFL) with an optical coating flaw from the FY06 PDS campaign in the beam. The red dashed line shows the propagation distance at which bulk damage was observed in the WFL. The green line shows the calculated peak intensity using the single wavelength (3ω only) model. The peak intensity produced by this calculation is not believed to be large enough to produce bulk damage. The blue line is a similar calculation using all three wavelengths. This calculation predicts sufficient peak intensity to produce bulk damage in agreement with the observation on PDS.

The three wavelength model has been used in subsequent calculations and is currently used in a production tool that accepts or rejects optical flaws on optics being prepared for NIF.

3) **Incorporate upgraded propagation codes and define optics specifications**

An original intent of this LDRD was to upgrade the propagation and damage models to allow more accurate prediction of performance on larger-aperture laser systems. Based on our observations in FY06, it became clear that improved metrology (an input to the damage model) and detailed optics specifications for each optic in the final optic package were equally important. The methodology required:

A) building an engine around the newly upgraded propagation code
B) creating a methodology to provide the needed PSDI phase files
C) benchmarking a library of defects from PDS that did and did not cause damage in the PDS 06 campaign against calculations using the new propagation code with input phase screens for the flaws provided by the PSDI measurements

A) <u>Build an engine around the upgraded propagation code</u>
Particular attention was paid to coating flaws, since downstream intensification due to these flaws was determined to be the primary source of optical damage in the PDS 06 campaign. While it was known that the morphology of coating flaws was not simple, it was hoped that parametric studies using Prop-based laser models and damage initiation rules could find a one-dimensional (or two- at most) physical property of the flaw that could be used to define a specification. It became apparent, however, that such a property could not be identified. It also became apparent that the newly installed Phase-Shifting Diffraction Interferometer (PSDI) was critical in the characterization of the coating flaws, since enhanced Prop models using PSDI-generated phase and amplitude masks were reliably (post-) predicting the PDS damage results. Attention then quickly turned to using the PSDI data to make real-time Prop runs and developing a specification based not on a physical characteristics of the flaw, but on the likelihood of downstream damage initiation from the flaw, due either to high intensity or high fluence contributions.

These real-time propagation runs have been realized in a new application called FOAQual (Final Optics Qualification). The application utilizes phase and intensity screens measured by PSDI, fluence and intensity files generated from PROP, damage initiation rules $\rho(\phi)$ (where ρ is the damage density at fluence ϕ), the damage initiation integral $N=\iint\rho(\phi)dxdy$, and pre-defined specifications. The damage initiation rules are based on a combination of off-line damage tests, on-line NEL results and, as described below, rely heavily on the PDS 06 experience.

B) <u>Create a methodology to provide the needed PSDI phase files</u>
Although reliably characterizing and setting specifications for flaws is a major part of the goal to eliminate problematic flaws on the final optics, an equally important part is the initial screening or identification of these flaws so that they can be subjected to the specification in the first place. PSDI has become a powerful tool to provide input to the damage model, but its small field of view requires some other tool to identify sites to be measured. Two types of large-aperture scanning tools are being used:

i) Reflected light

In the case of sol gel AR coating flaws, imaging the coated optic under illumination with a full-aperture, diffuse-light box (FADLiB) has proven to be quite effective.[18] This simple technique was implemented on an automated stage and integrated with OI (optics inspection) software to automatically detect phase perturbations and drive the stage to the correct location to allow acquisition of a high-resolution PSDI image. All optics for the FY07 PDS campaign were screened with this tool.

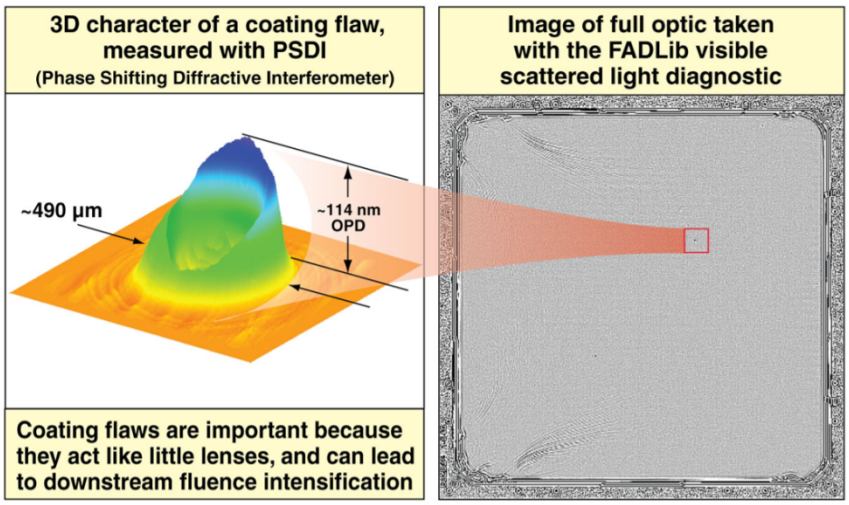

Figure 22: FADLib image of a 43x43cm optic (on the right) and the PSDI image of a specific defect detected on the surface of the optic.

ii) Transmitted light

An older technique, IMS (inclusion mapping system) uses transmitted light to detect defects.[19] This technique backlights the optic with a narrow-band-filtered white light source and measures the amplitude at multiple planes downstream of the optic. Phase unwrapping techniques then allow calculation of the phase and amplitudes of defects inside or on the optic. This technique is relatively easy to use at low resolution with a large field of view, making it a useful scanning tool for phase defects.

This technique has been used extensively in the past to detect bulk inclusions in fused silica, but was not used for the initial screening of optics for the PDS 06 or 07 campaigns. It became clear after the first few shots of the PDS 07 campaign (explained below), that IMS mapping should be a core part of flaw management. It was used on all subsequent TCVWs and 1ωCPPs for PDS and NIF.

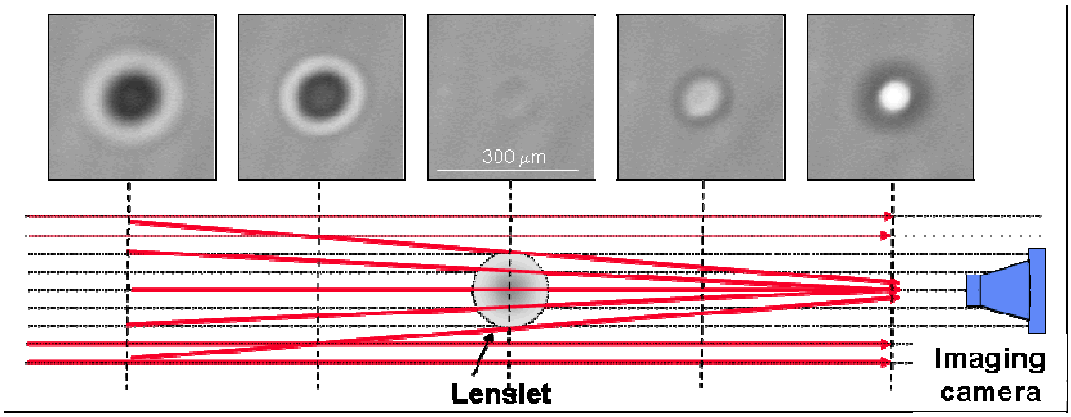

Figure 23: Images at multiple planes taken via IMS using filtered white light.

C) Benchmark PDS defect library to define flaw specifications

PSDI phase files taken in this manner were combined with PDS06 shot and damage data to set the damage-initiation-based specifications. A summary of this data is shown in Figure 24.

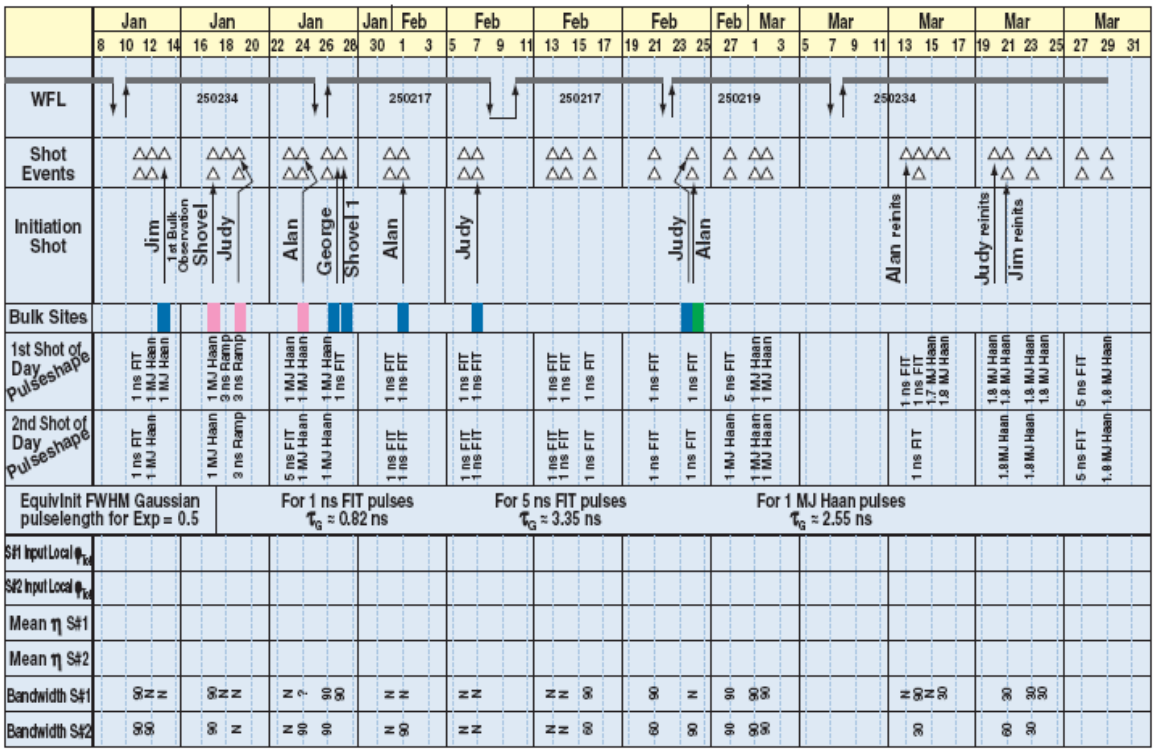

Figure 24. Overview of the FY06 PDS shot campaign (ignores early shots)

Since the optics used in this campaign had flaws that both did and did not lead to downstream damage under known irradiation conditions, they were prime candidates for flaw specification benchmarking. It was observed that damage was initiated both at high intensity (in the bulk of the WFL), and at high fluence (at the exit surface). It was agreed that a damage-based specification should cover both instances. PSDI data was taken at

18 coating flaw locations exposed to laser light on the PDS THG (634002) and the SHG (624002). Of these 18 defects, 5 were observed to lead to damage at the WFL. These flaws were given nick-names: Alan, Judy, Jim, Mike, and Pam. PSDI phase images of these 5 flaws are shown in Figure 25.

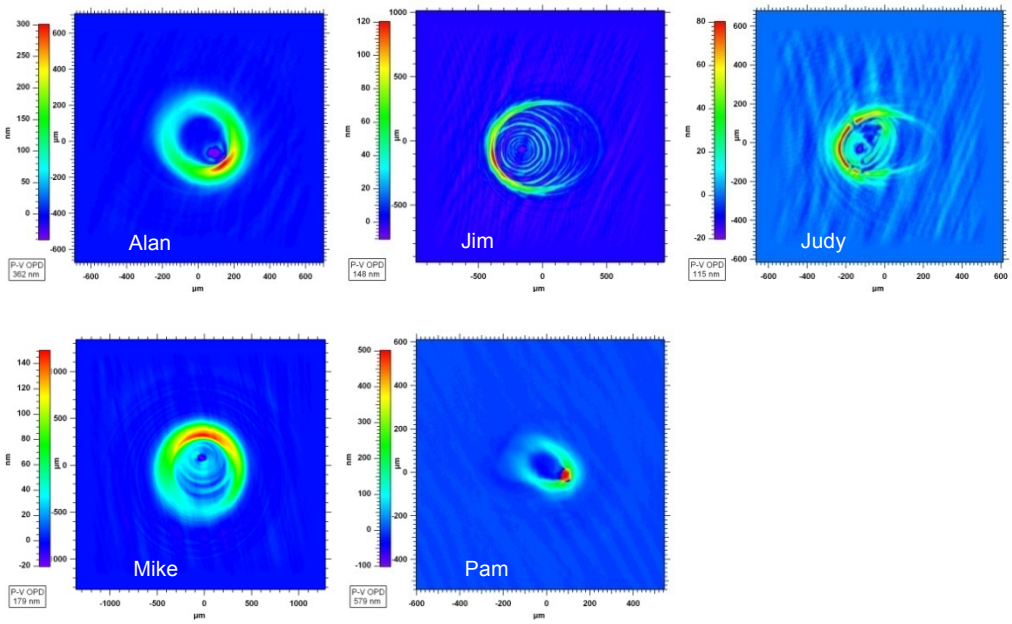

Figure 25. PSDI images of the 5 crystal coating flaws that led to downstream damage during the PDS 06 campaign.

All 18 flaws were run through enhanced Prop codes to determine the peak intensification inside the WFL, as well as the damage initiation integral at the exit surface. N was computed using the latest 3ω rho-of-phi-at-high-phi rule. Calculations that incorporated total fluence were also performed but did not benchmark the PDS data as satisfactorily as the 3ω-only calculations. This is believed to be true because the benchmarking value of N was deliberately set to a small value, ~0.03, where multiple wavelength effects are expected to be small. The results for the PDS FY06 optical configuration are show in Table 1.

			FIT		Haan				WFL	WFL
			1-ns	1-ns	1.8 MJ	1.8 MJ	Max	Max	surface	bulk
	Flaw ID	Surface	I_{pk}	N	I_{pk}	N	I_{pk}	N	damage?	damage?
1	Alan	SHG In	248.20	1.389	9.85	2.060	248.20	2.060	yes	yes
2	Jim	THG Out	175.30	1.334	26.19	1.828	175.30	1.828	yes	yes
3	Judy	THG Out	31.61	0.310	5.90	0.071	31.61	0.310	yes	yes
4	Pam	SHG In	11.50	0.060	7.25	0.365	11.50	0.365	yes	no
5	Mike	THG In	10.11	0.109	4.88	0.353	10.11	0.353	yes	no
6	634-F	THG Out	12.40	0.065	4.65	0.012	12.40	0.065	no	no
7	624-H	SHG Out	10.21	0.021	4.71	0.029	10.21	0.029	no	no
8	25150	THG In	10.27	0.014	4.01	< 0.001	10.27	0.014	no	no
9	21770	THG In	8.82	< 0.001	3.74	< 0.001	8.82	< 0.001	no	no
10	634-D	THG In	9.68	0.032	4.53	0.187	9.68	0.187	no	no
11	13210	THG In	9.57	0.013	3.81	< 0.001	9.57	0.013	no	no
12	25650	THG In	8.58	< 0.001	3.52	< 0.001	8.58	< 0.001	no	no
13	7390	THG In	6.14	< 0.001	3.49	< 0.001	6.14	< 0.001	no	no
14	6450	THG In	6.01	< 0.001	3.27	< 0.001	6.01	< 0.001	no	no
15	624-G	SHG Out	5.79	< 0.001	3.29	< 0.001	5.79	< 0.001	no	no
16	22490	THG Out	5.81	< 0.001	3.23	< 0.001	5.81	< 0.001	no	no
17	634-H	THG Out	5.20	< 0.001	2.83	< 0.001	5.20	< 0.001	no	no
18	634-E	THG Out	4.20	< 0.001	2.40	< 0.001	4.20	< 0.001	no	no

Table 1. Prop predictions for the 18 crystal coating flaws studied on PDS. Only 3ω fluence was considered for the damage integral calculations. The 1-ns FIT pulse assumes 3.5 GW/cm^2 drive intensity.

Based on the data in Table 1, the following limits were adopted:

· Peak Intensity limit: $I_{pk} < 25$ GW/cm^2
· Damage integral limit: $N < 0.1$

These limits include some margin for uncertainties, such as beam contrast and crystal non-homogeneities, which are not included in the calculation. In other words, although this data may suggest a damage integral limit of closer to N = 0.2 and peak intensity closer to $I_{pk} = 100$ GW/cm^2, it was not deemed prudent to set specification limits there, but at values with a reasonable amount of margin built in. These limits are not the final specifications however, since allowance for a moveable WFL needs to be incorporated. Setting N=0.03 compensates for the fact that the WFL may be moved over a range of +/- 40mm shot-to-shot.

Thus the strategy for qualifying flaws (other than those already covered by vendor specs.) on the final optics consists of:

1) Using the FADLiB or IMS image to identify the locations of potentially lethal flaws
2) Acquiring PSDI phase and amplitude screens at these flaw locations
3) Running FOAQual to determine whether the flaws pass or fail a specification based on the likelihood of downstream damage initiation

Verification of Flaw Management Strategy: FY07 PDS Campaign

The FY07 PDS campaign had three phases:

1) verify operational and performance qualification for the new IOM hardware/design,
2) verify laser and optic performance for the NIF 3ω design baseline, and

3) demonstrate laser and optic performance for proposed 2ω missions.

Figure 26 summarizes the campaign energetic. Details of the laser performance are summarized elsewhere.[5,6,7]

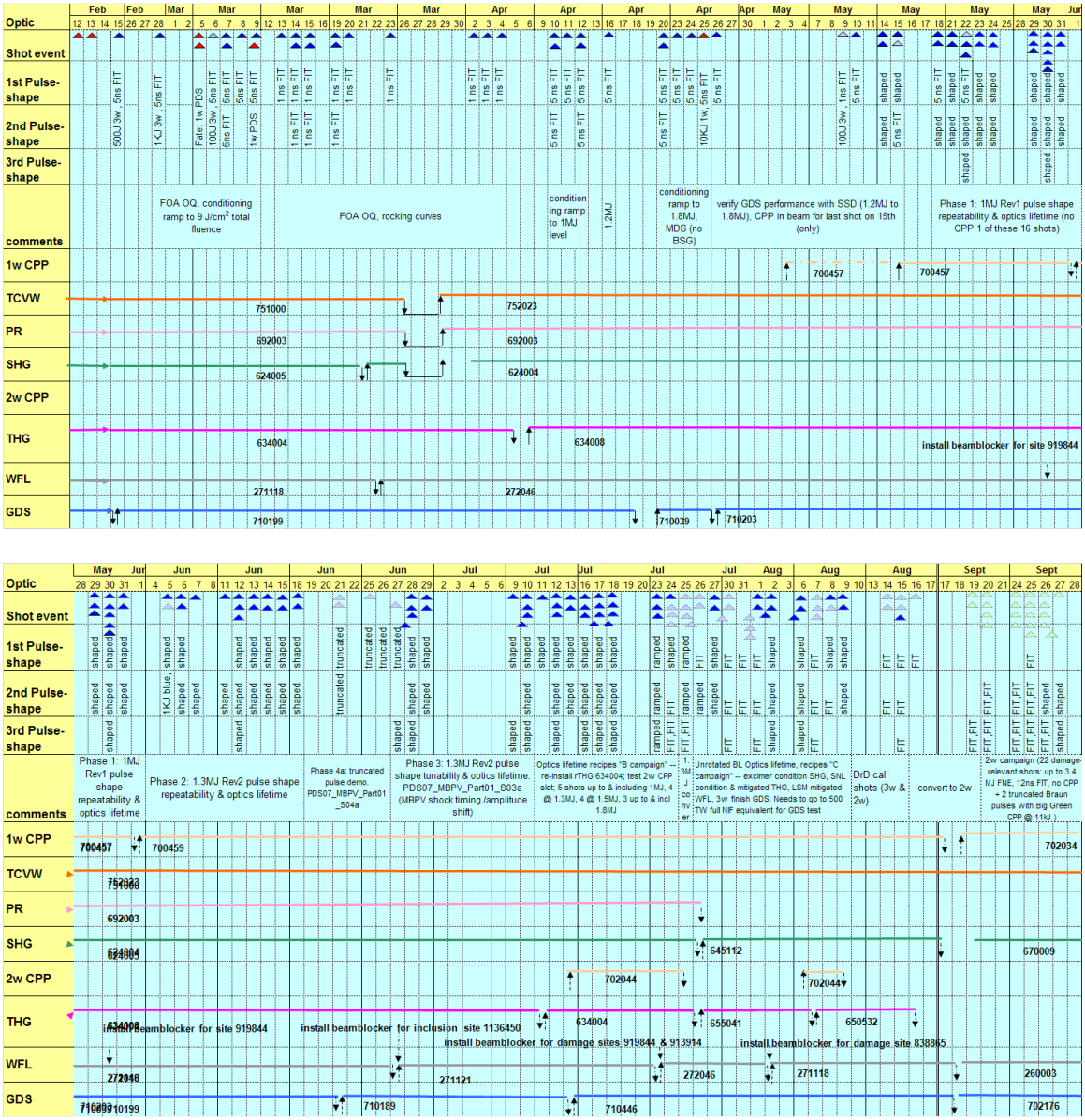

Figure 26: Twenty four different large optics (CPP, TCVW, PR, SHG, THG, WFL, GDS/MDS) were fielded during the PDS 07 campaigns.

The PDS 07 campaigns provided the opportunity to verify the robustness of the new IOM optical design (optic spacings) and optics flaw management strategy. 160 damage-relevant 3ω and 2ω shots were fired on 24 different large optics; 138 3ω drive shots were executed with a cumulative 3ω energy of 719kJ followed by 22 shots with cumulative 273kJ 2ω drive energy. (Figure 27)

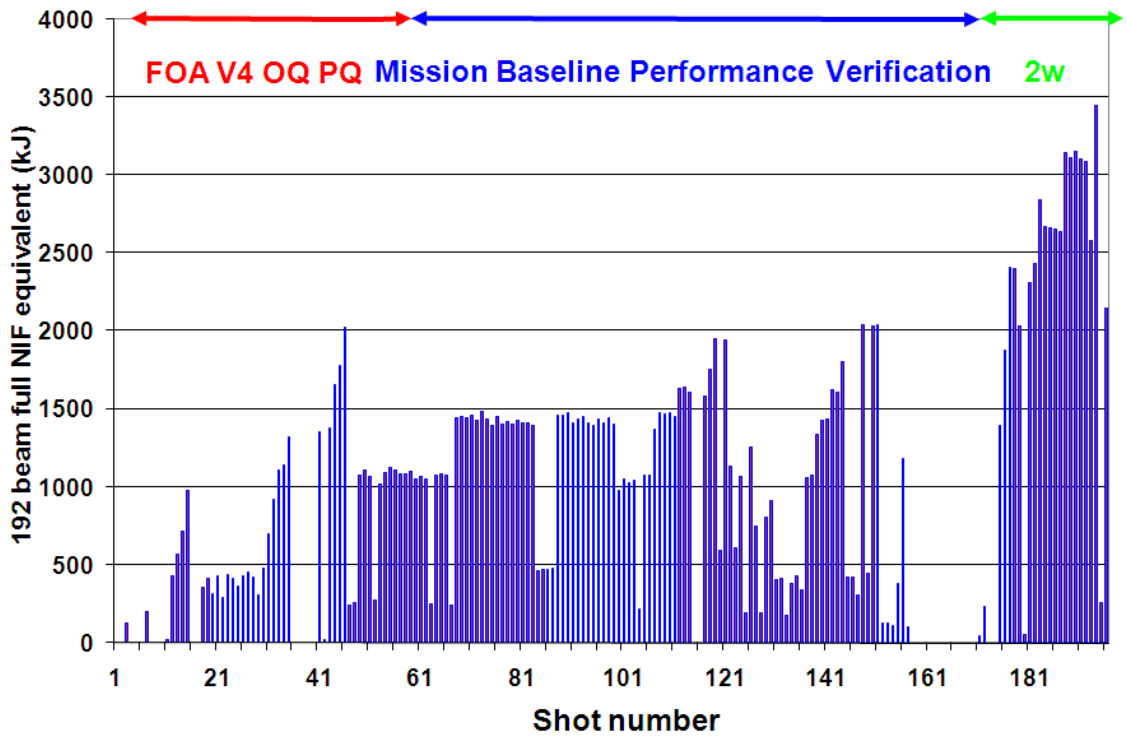

Figure 27: One hundred thirty-eight damage-relevant 3ω shots plus twenty two damage relevant 2ω shots were fired during the PDS 07 campaigns

Through the entire campaign, there was only one observation of fratricide-induced damage: inadequate metrology allowed fielding of a TCVW with a surface flaw which initiated damage at the WFL during low energy, 1 ns square pulses on the 6th 3ω shot of the campaign.

The TCVW-induced WFL damage was costly in terms of time and optics change-outs, but it provided a valuable opportunity to test the new models and flaw specifications. It has been known for some time that the Corning 7980, the type of fused silica historically used on large lasers and used throughout the 1ω portion of NIF, contains bulk inclusions (fully or partially dissolved refractory brick) that can act like lenslets.[19] For this reason, PDS (and NIF) have replaced Corning 7980 in the final optics with low-inclusion silica manufactured using the same process as for material destined to become fiber optics. Because of this change in silica, the initial TCVW for the FY07 PDS campaign was not mapped with IMS despite the fact that the new final optics optical configuration increases the vulnerability of the WFL to phase defects of this type located in the vicinity of the TCVW and 1ωCPP.

The initial TCVW was mapped with FADLib, but no surface flaws were observed that failed the new flaw specifications. The IMS maps for this window—taken after removal from PDS—and its replacement are shown below in Figure 28.

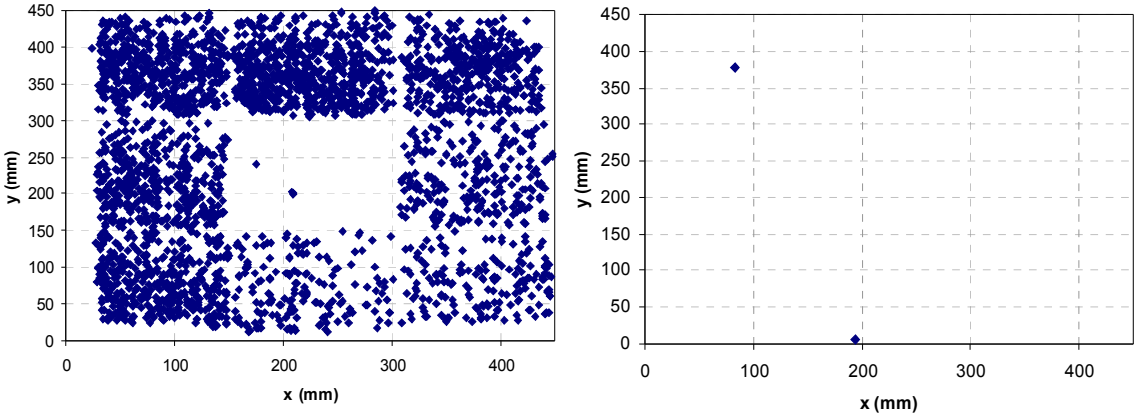

Figure 28: IMS maps for TCVW 751000 on left and 751023 on right. The grid and empty middle section on 751000 are artifacts caused by failure of the OI software to properly handle the >3000 phase objects on this optic—compared to two on the replacement window.

As shown in Figure 28 above, the initial PDS TCVW contained a large number of a new type of defect that is invisible to FADLib, and therefore passed the initial PDS screening. The defects are very difficult to detect visually. Enough were apparent that the LLNL scratch/dig inspections had noted "numerous digs", but none that failed the vendor scratch/dig specification.

Based on the IMS mapping, PSDI was done on the defects with the largest size and OPD (optical path difference). Figure 29 below shows the PSDI for the site that was precisely upstream of the observed WFL damage.

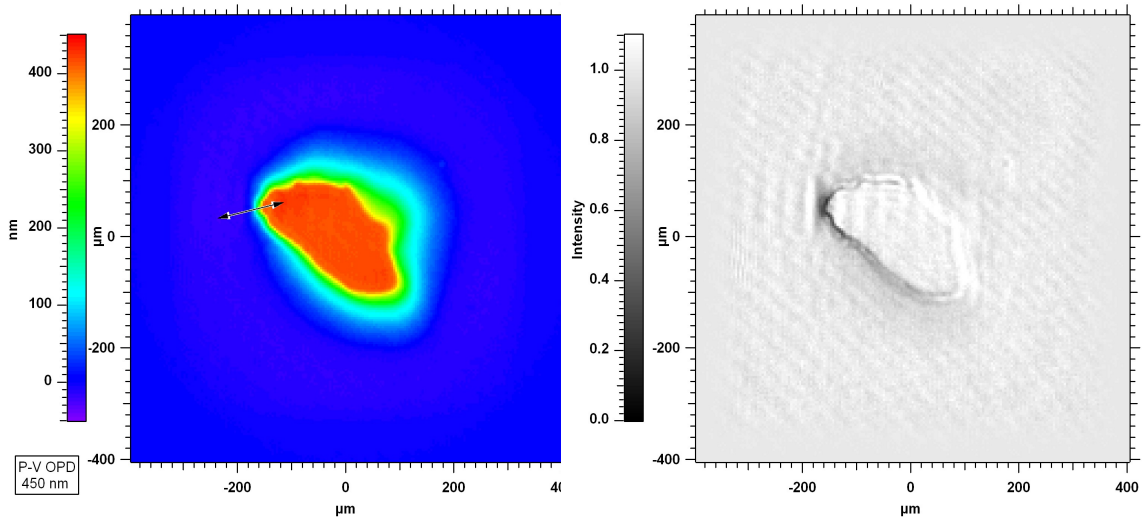

Figure 29: PSDI of the TCVW flaw that induced damage on the PDS WFL at only 3 J/cm^2, 3ω. The flaw, on the output surface of TCVW 751000, is ~300 µm laterally, ~1 µm high and has an OPD of 450nm.

The flaw was invisible to FADLib because it did not perturb the sol gel AR coating sufficiently to affect the reflected light. Once found, the flaw and its >3000 siblings on

this window were quickly identified as a defect caused in the finishing process of the TCVW. The finishing window had achieved the NIF transmitted wavefront requirement by ion-figuring the output surface to compensate for material inhomogeniety. Apparently debris from a dirty chamber that fell on the optic acted as localized masks, resulting in flaws such as the high flat spot shown in Figure 29 above. Discovering this flaw on PDS was extremely helpful since all of the optics finished in this manner can now be re-polished to eliminate this class of defects rather than discovering them on NIF through WFL damage.

Once the offending flaw was identified, it was run through FOAQual to see whether damage would be expected. The local fluence based on the PDS near field maps was in the range of 2.9-3.2 J/cm^2. FOAQual showed damage would not be expected at 2.5 J/cm^2, was likely at 3 J/cm^2 and was assured at 3.5 J/cm^2. FOAQual failed the optic for use on PDS. The replacement TCVW 751023 showed two sites (Figure 28), but neither failed the FOAQual spec.

Thus the recent TCVW-induced WFL damage demonstrates that the methodology described above should be effective at eliminating fratricide in the final optics package—as long as adequate metrology is done in advance. A powerful lesson learned is the recognition that each large aperture optic is unique and we should expect to continue to find new types of flaws showing up. The best defense against modulation-induced fratricide is to use all pre-installation metrology possible. In this case, both FADLib and IMS must be used to detect flaws in both transmitted and reflected light.

Figure 30. PFODI images of a wedged focus lens from PDS 06 and a different lens from PDS07 after a similar series of shots up to 8.5 J/cm^2 3ω.

The elimination of flaw-induced damage (improved optics spacings, improved flaw specifications) and surface-quality related damage (improved polishing quality of the WFL) yielded a nearly damage-free WFL even after 40 shots, averaging 6.1 J/cm2, and

ranging from between 4.8 and 9.5 J/cm2 (1.0 and 2.0 MJ NIF-equivalent). The PDS07 WFL shown above had only three damage sites >40 μm.

Early in the PDS07 campaign, we once again observed laser damage which followed the arc of the GDS grating. This time, the damage was faintly observed after the final "1MJ" conditioning shot (5.4 J/cm^2 3ω, 5ns FIT), and then grew catastrophically when the 3ω fluence was increased by 20% to 6.2 J/cm^2. Not only did this damage occur at much lower energy than was observed in the PDS 06 campaign, it produced substantial bulk damage as well as surface damage along the grating. It is suspected that changes in the incident angle and focal length of the beam sampling grating to facilitate ghost management in the new IOM design resulted in subtle changes in the grating which amplified the non-linear processes that were occurring in the final shots of the PDS 06 campaign.

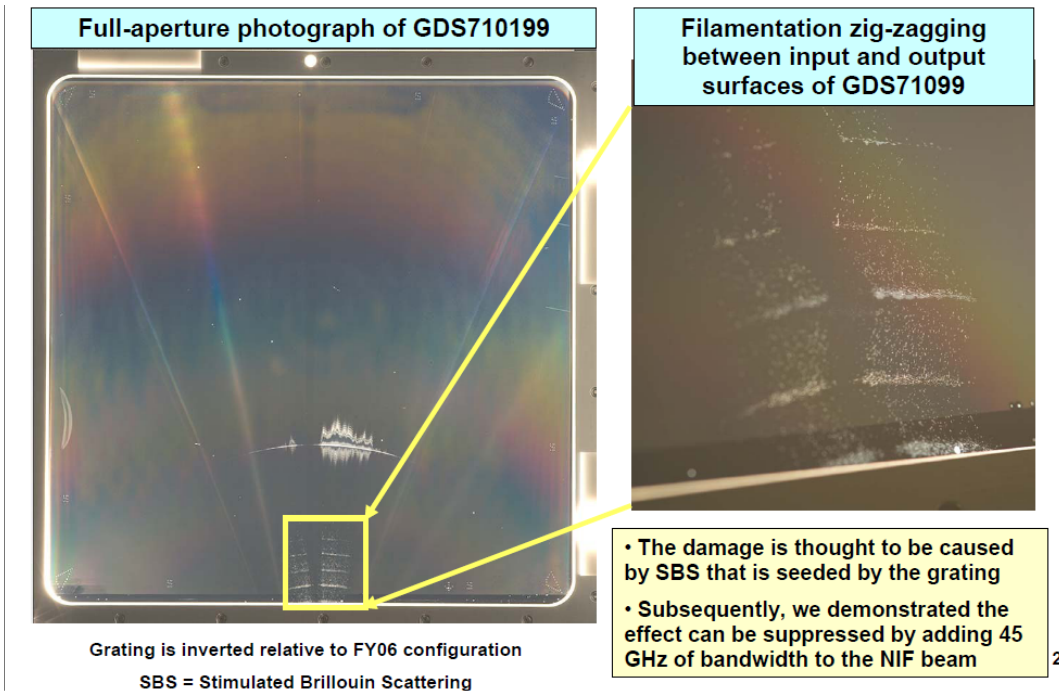

Figure 31: Full aperture backlit image of the GDS showing damage following the 6.2 J/cm2 5ns 3ω pulse during the PDS07 campaign. Insert shows damage planes in the bulk of the optic which zig-zag between the output surface (containing the beam sampling grating) and the input surface (no grating) along grating lines.

As can be seen in Fig. 31, the bulk damage occurred along planes suggesting a sheet of light totally internally reflecting between the two surfaces of the optic.
The zig-zag reflected path is hypothesized to have provided the high IL product (intensification) required to create filamentary damage. The observed damage is consistent with a qualitative model for damage from SBS.[20] This would also explain the pattern of surface damage seen in FY06 – which mirrored the grating pattern on the un-patterned input surface of the optic. To suppress the SBS, 45 GHz additional SSD (spectral smoothing by dispersion) bandwidth was added to the pulse conditioning. This minimum bandwidth has become a machine safety requirement, and has prevented

recurrence of GDS damage on PDS and on NIF, including shots which delivered the equivalent of 2.0MJ 3ω energy to target chamber center and 3.5 GW/cm^2 peak 1ω intensity into the package.

Key conclusions from the PDS 07 Campaign

1) The flaw management strategy—a combination of the new flaw specifications applied to the optics and the modified optics configuration—worked extremely well
2) The novel grating-specific damage on the GDS was completely eliminated by increasing SSD by 45 GHz, lending credence to the hypothesis that the GDS damage was due to SBS.
3) There was no damage initiation observed during the high energy 2ω campaign shots. This was consistent with expectations from off-line experiments.

FY08 Validate damage models, tools during NIF Commissioning

In FY08, the FODI instrument (Figure 32), an optical duplicate of the PFODI system, was commissioned at Target Chamber Center (TCC). The first twenty IOMs were fielded on the NIF Target Chamber, populated with optics and inspected by FODI to complete the commissioning shot readiness activities. The first eight beams were successfully commissioned through 5.6kJ, 3ω (operationally qualified) and two of these beams were operated to full NIF specifications – 1.8MJ FNE, shaped pulses (performance qualified) in late spring, 2008. Truth optics and VIEW microscopy of damage sites from optics removed from NIF during these campaigns have confirmed that FODI meets its requirements for *in situ* damage detection and sizing.

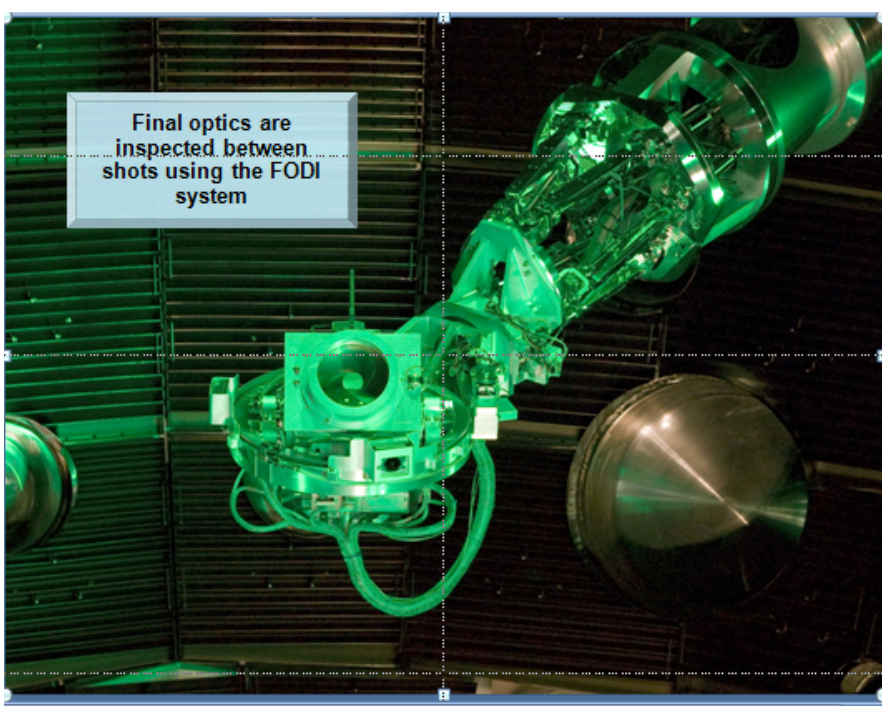

Figure 32. FODI fielded on the NIF Target Chamber at the end of the FODI DIM.

As shown in Figure 33, a total of 34 shots were taken through the two PQ beamlines in FY08. Edge-lit FODI images were collected at extended intervals during the first 17 shots, and after every shot above 1 MJ FNE. No fratricide events were observed in the IOMs.

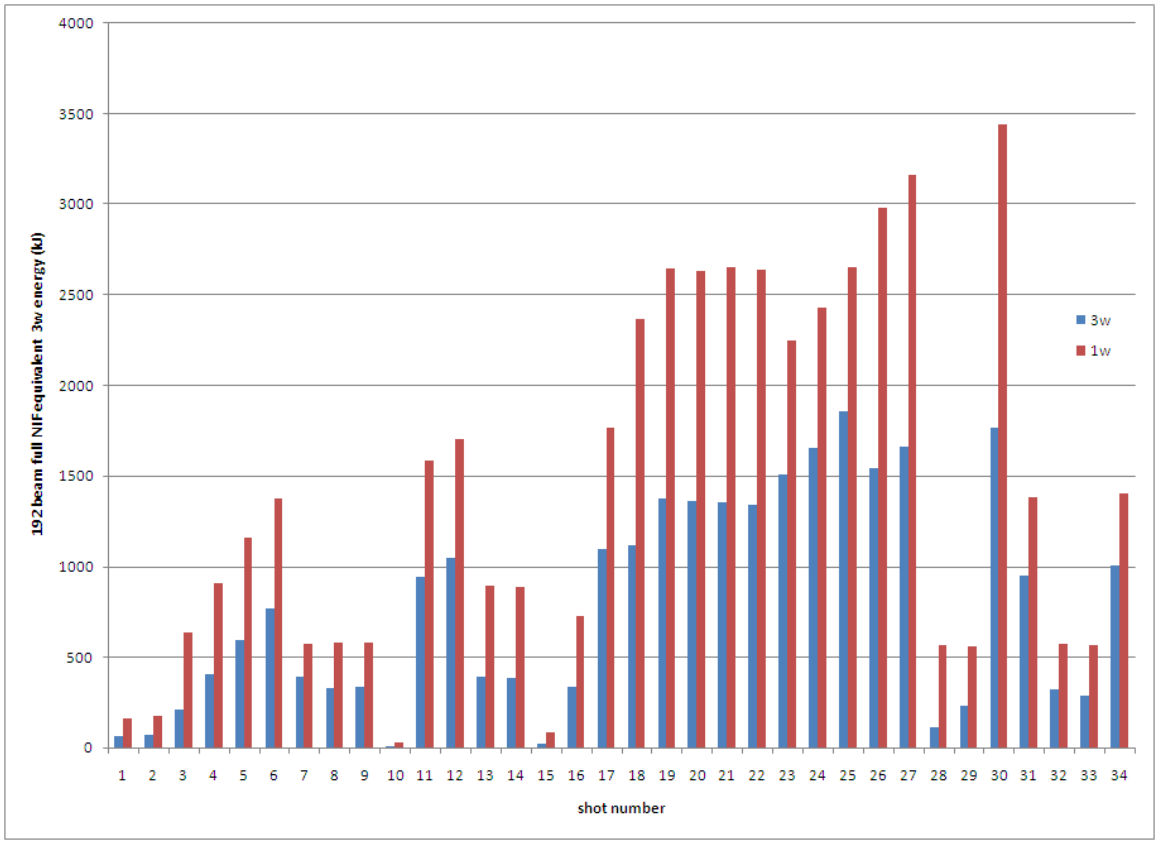

Figure 33. Energy (Joules 3ω) for the first 34 performance qualification shots on two beamlines in Bundle 34 on the NIF Target Chamber.

Detailed analyses of the PDS07 data provided the first damage initiation density rules under NIF-relevant conditions for full-size optics. Off-line measurements have been limited by test laser pulse shape and optic test area and quality – it has previously been impractical to test sufficient area on small-beam lasers or to fabricate representative sub-scale test optics using NIF-production processes. Comparison of damage density rules generated during pre-initiation of wedged focus lenses compared to observations of initiation density observed on PDS optics pointed out that the pulse-scaling used for the pre-initiation laser was over-stating the damage equivalent fluence. Once this fluence correction was made, the damage initiation models agreed well with observed initiations on PDS, as seen in Figure 34. This methodology has been successfully applied to other optics which were not pre-initiated in our off-line laboratory, such as the GDS and THG, with similar success.

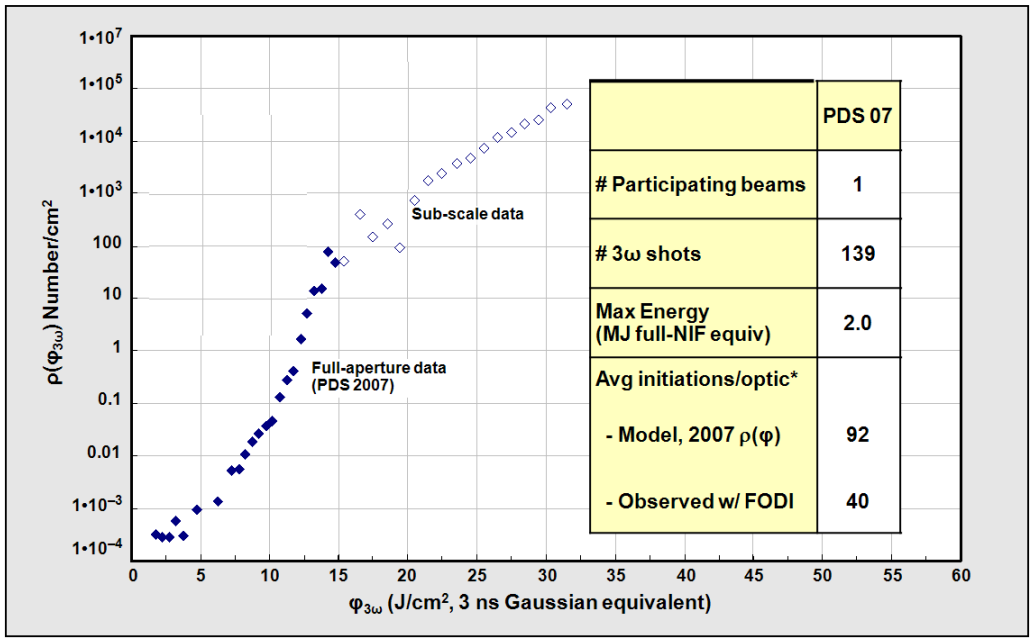

* Wedged focus lens

Figure 34. The damage density at low fluence ρ(Φ) derived from PDS 07 campaign is combined with the damage density observed at high fluence derived from sub-scale optics to produce a damage initiation rule which can predict the expected initiation for a future shot campaign. Here, we compare the FODI observed results to the prediction for the PDS 07 campaign.

Analysis of the PDS07 fused silica growth data generated greatly improved shot-to-shot statistics, leading to an exponential distribution of growth alphas as a function of fluence. The mean alpha from the PDS data was unchanged from the off-line model – which is based on the total fluence (1ω + 3ω) incident on the damage site. Figure 35 shows excellent agreement between predictions from the new growth model with the observed PDS data for over 150 damage sites exposed to 15 consecutive shots at ~ 10kJ/beamline total energy. The error bars are the 1-sigma distribution based on the exponential distribution. This alpha distribution will be incorporated into the damage growth calculations used to determine optics maintenance demand.

Change in diameter on a single shot is given by:

$$D = D_0 \cdot e^{\alpha(\varphi)}$$

where α is an exponentially distributed random variable with mean value:

$$\bar{\alpha}(\varphi) = 0.038 \cdot (\varphi_{Total} - \varphi_{thresh})$$

4.5 J/cm²

$$\varphi_{Total} = \varphi_{1\omega} + \varphi_{2\omega} + \varphi_{3\omega}$$

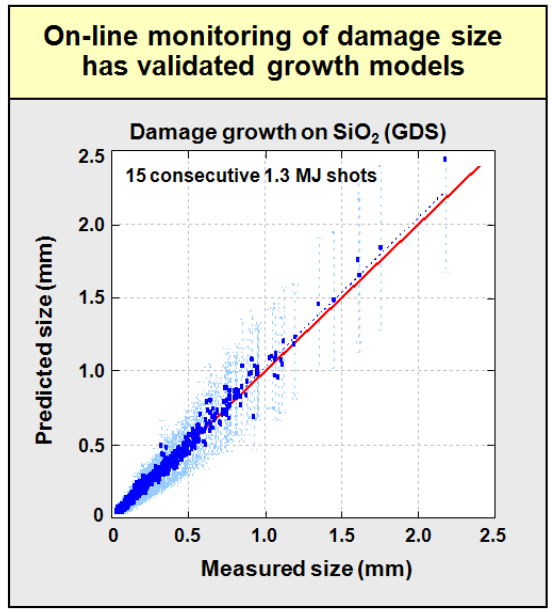

Figure 35: Comparison of the predicted vs measured damage site diameter for GDS exit surface damage sites exposed to 15 consecutive 1.3MJ FNE shaped pulse shots on PDS.

Analysis of the PDS07 crystal growth data has proven more problematic, in part due to the fabrication methodology which can introduce digs and other high density flaws on the input surface of the crystal. While exponential growth is the norm for fused silica exit sites, it is the exception for THGs. Initial efforts to use machine-learning to differentiate input from exit surface sites based on FODI signature and growth habit have shown limited success[21]. This well characterized (energy, microscopy) PDS data set will be invaluable for benchmarking future growth prediction algorithm improvements.

Exit Plan

This work will add substantially to the knowledge base for integrated large aperture systems for optical materials under intense laser illumination (i.e. fusion-class lasers systems) and allow us to improve and validate our theoretical and stochastic models. This work supports NNSA/LLNL mission needs in Stockpile Stewardship because the safety and reliability of the nuclear stockpile in the absence of testing will rely heavily on the experimental data from fusion-class laser systems to validate complex coupled-physics computer simulations.

We have already applied similar modeling, pre and post characterization and extensive shot-to-shot monitoring during the full bundle (34PQ) performance campaign completed in mid-October, 2008 and during commissioning of the first 111 beams in December, 2008. Figure 36 shows good agreement between our fused silica initiation model and observations during these campaigns.

	Campaign		
	PDS 07	96 Beam OQ	Bundle PQ
# Participating beams	1	111	8
# 3ω shots	139	12	23
Max Energy (MJ full-NIF equiv)	2.0	1	1.8
Avg initiations/optic*			
- Model, 2007 ρ(φ)	92	8	27
- Observed w/ FODI	40	18	52

Figure 36. FODI observations of damage initiation on the first 111 NIF beamlines is within ~2x of damage models developed from the PDS07 results.

As commissioning of the remaining 81 NIF beamlines is completed and NIF operations begin, the damage models, flaw specifications and monitoring techniques developed in this project will be improved with data from an even larger set of optics. Ultimately, these tools will become core to the optics loop operations required to maximize the return on the NIF capital investment by maximizing the delivered data per operating dollar on a rolling basis.

Summary

We evaluated large optics at full aperture over a wide range of fluence and intensity, with unconverted light present and with statistical fluctuations typical of large aperture lasers. Specialized optomechanical hardware which edge-illuminated the optics was coupled with a new flaw inspection system and extensive laser diagnostics in an existing large aperture laser system called the Precision Diagnostic System (PDS) to allow *in situ* analysis of damage initiation and growth. Nearby upstream (-z) flaws on neighboring optics were found to be major contributors to optics damage. Based on results of the initial experiments, improvements were made in the optical configuration and in the optics themselves that significantly reduced their susceptibility to laser-induced damage. The concepts for optical configuration, flaw specifications for the final optics and the *in situ* inspection hardware and software have been implemented on NIF with excellent results.

Acknowledgements

We wish to acknowledge the many co-workers on NIF who contributed ideas, suggestions or analysis to this work and also the engineering team who implemented the concepts developed here.

References

1. "Laser heating of free electrons in wide-gap optical materials at 1064nm," X.A. Shen, S.C. Jones, P. Braunlich, Phys. Rev. Let, **62**, 23, 2711 (1989)
2. "Recent Progress on Laser-Induced Modification and Intrinsic Bulk Damage of Wide-Gap Optical Materials", Optical Eng., **28**, No10, 1039 (1989)
3. "Growth of laser damage in SiO_2 under multiple wavelength irradiation," M. A. Norton, E. E. Donohue, M. D. Feit, R. P. Hackel, W. G. Hollingsworth, A, M. Rubenchik, M. L. Spaeth, November 1, 2005, Boulder Damage Symposium XXXVII, Boulder, CO, United States, September 19, 2005 through September 21, 2005, UCRL-PROC-216742.
4. "Laser Damage Growth in Fused Silica with Simultaneous 351 nm and 1053 nm irradiation," Mary A. Norton, Adra V. Carr, C. Wren Carr, Eugene E. Donohue, Michael D. Feit, William G.Hollingsworth, Zhi Liao, Raluca A. Negres, Alexander M. Rubenchik, P. J. Wegner, October 31, 2008, Boulder Damage Symposium, Boulder, CO, United States, September 22, 2008 through September 24, 2008.
5. "National Ignition Facility laser performance status," C.A. Haynam, P.J. Wegner, J.M. Auerbach, M.W. Bowers, S.N. Dixit, G.V. Erbert, G.M. Heestand, M.A. Henesian, M.R. Hermann, K.S. Jancaitis, K.R. Manes, C.D. Marshall, N.C. Mehta, J. Menapace, E. Moses, J.R. Murray, M.C. Nostrand, C.D. Orth, R. Patterson, R.A. Sacks, M.J.Shaw, M. Spaeth, S.B. Suttton, W.H. Williams, C.C. Widmayaer, R.K. White, W.T. Yang, B.M.Van Wonterghem, Applied Optocs, Vol. 46, No. 16, June 1, 2007.
6. "The National Ignition Facility 2007 Laser Performance Status," C.A. Haynam, R.A. Sacks, P.J. Wegner, M.W. Bowers, S.N. Dixit, G.V. Erbert, G.M. Heestand, M.A. Henesian, M.R. Hermann, K.S. Jancaitis, K.R. Manes, C.D. Marshall, N.C. Mehta, J. Menapace, M.C. Nostrand, C.D. Orth, M.J.Shaw, S.B. Suttton, W.H. Williams, C.C. Widmayaer, R.K. White, W.T. Yang, B.M.Van Wonterghem, The 5th International Conference on Inertial Fusion Sciences and Applications (IFSA2007), IOP Publishing, Juournal of Physics, Conference Series **112** (2008) 032004.
7. "Demonstration of high-energy 2ω (526:5nm) operation on the National Ignition Facility Laser System,"G. M. Heestand,* C. A. Haynam, P. J. Wegner, M. W. Bowers, S. N. Dixit, G. V. Erbert, M. A. Henesian, M. R. Hermann, K. S. Jancaitis, K. Knittel, T. Kohut, J. D. Lindl, K. R. Manes, C. D. Marshall, N. C. Mehta, J. Menapace, E. Moses, J. R. Murray, M. C. Nostrand, C. D. Orth, R. Patterson, R. A. Sacks, R. Saunders, M. J. Shaw, M. Spaeth, S. B. Sutton, W. H. Williams, C. C. Widmayer, R. K. White, P. K. Whitman, S. T. Yang, and B. M. Van Wonterghem, p. 3494, APPLIED OPTICS / Vol. 47, No. 19 / 1 July 2008
8. "Final optics damage inspection (FODI) for the National Ignition Facility," A. Conder, T. Alger, S. Azevedo, J. Chang, S. Glenn, L.Kegelmeyer, J. Liebman, M.

Spaeth, P. Whitman, November 12, 2007, UCRL-PROC-236458, Boulder Damage Symposium Boulder, CO, United States, September 24, 2007 through September 26, 2007.
9. "Laser Performance Operations Model (LPOM): A tool to automate the setup and diagnosis of the National Ignition Facility," M. Shaw, W. Williams, R. House, C. Haynam, August 2005, UCRL-ABS-213999.
10. "LPOM: A Tool to Automate the Setup and Diagnostics of the National Ignition Facility", M. J. Shaw, R. K. House, W. H. Williams, C. A. Haynam, UCRL-ABS-228587, March 2, 2007.
11. "NIF final optics system: frequency conversion and beam conditioning," P. Wegner, J. Auerbach, T. Biesiada, S. Dixit, J. Lawson, J. Menapace, T. Parham, D. Swift, P. Whitman, and W. Williams, UCRL-CONF-155817, January 28, 2004, SPIE Photonics West, San Jose, California, January 24-29, 2004.
12. "Design of an Illumination Technique to Improve the Identification of Surface Flaws on Optics," Rahul Prasad, Michael Bernacil, John Halpin, John Peterson, Steve Mills, and Richard P. Hackel, SPIE **5647**, 421, 2004.
13. "MRF Applications: On the Road to Making Large-Aperture Ultraviolet Laser Resistant Continuous Phase Plates for High-Power Lasers," J. A. Menapace, P. J. Davis, W. A. Steele, M. R. Hachkowski, A. Nelson, K. Xin, UCRL-CONF-225806, October 26, 2006, Boulder Damage Symposium, Boulder, CO, United States, September 25, 2006 through September 27, 2006.
14. "Theory and application of point-diffraction interferometers," R. N. Smartt and W. H. Steel, In Jpn. J. Appl. Phys. 14, 351-356, 1975.
15. "Point diffraction interferometery at soft x-ray wavelengths In Soft X-Ray Projection Lithography," G. E. Sommargren and R. Hostetler, eds. A. M. Hawryluk and R. H. Stulen, Vol. 18 of OSA Proceedings Series Optical Society of America, Washington, D.C., 1993, p. 100.
16. United States Patent 5,548,403, G. Sommargren, August 20, 1996.
17. "Simulations of 3ω Beam Filamentation in the Beamlet Focus Lens and General Comments on Filamentation Theory," M.A. Henesian, LS&T-LMO-96-001, presented at Second International Conference on Solid State Lasers for Application to Inertial Confinement Fusion (ICF), October 22-25, 1996, Paris, France.
18. Technique for rapid detection of light intensifying defects on ICF laser optics," Frank L. Ravizza, Michael C. Nostrand, Ruth A. Hawley and Michael A. Johnson, May 16, 2008, Boulder Damage Symposium XL, Boulder, CO, United States, September 22, 2008 through September 24, 2008, LLNL-ABS-403951
19. "Correlation of Laser-induced Damage to Phase Objects in Bulk Fused Silica," M.C. Nostrand, C. J. Cerjan, M. A. Johnson, T. I. Suratwala, T. L. Weiland, W. D. Sell, J. L. Vickers, R. L. Luthi, J. R. Stanley, T. G. Parham, C. B. Thorsness, Proceedings of SPIE Vol. **5647**, 233 (2004).
20. Private communications with J. Trenholme, LLNL.
21. "Defect Classification Using Machine Learning," Adra Carr, L. Kegelmeyer, Z. M. Liao, G. Abdulla, D. Cross, W.P. Kegelmeyer, F. Ravizza, and C. W. Carr, May 16, 2008, Boulder Damage Symposium XL, Boulder, CO, United States, September 22, 2008 through September 24, 2008, LLNL-PROC-408339.